MARYLAND

COLLEGE PARK CAMPUS

POLLUTION ERROR IN THE *h*-VERSION OF THE FINITE ELEMENT METHOD AND THE LOCAL QUALITY OF THE RECOVERED DERIVATIVES

by

I. Babuška
T. Strouboulis
S. K. Gangaraj
C. S. Upadhyay

1995013 079

INSTITUTE FOR PHYSICAL SCIENCE
January 1995
AND TECHNOLOGY

REPORT DOCUMENTATION PAGE		READ INSTRUCTIONS BEFORE COMPLETING FORM
1. REPORT NUMBER Technical Note BN-1180	2. GOVT ACCESSION NO.	3. RECIPIENT'S CATALOG NUMBER
4. TITLE (and Subtitle) Pollution Error in the h-Version of the Finite Element Method and the Local Quality of the Recovered Derivatives		5. TYPE OF REPORT & PERIOD COVERED Final Life of Contract
		6. PERFORMING ORG. REPORT NUMBER
7. AUTHOR(s) I. Babuska[1] - T. Strouboulis[2] - S. K. Gangaraj[2] - C. S. Upadhyay[2]		8. CONTRACT OR GRANT NUMBER(s) [1]N00014-90-J-1030 & CCR-88-20279/NSF [2]See Page 1
9. PERFORMING ORGANIZATION NAME AND ADDRESS [1]Institute for Physical Science and Technology University of Maryland College Park, MD 20742-2431		10. PROGRAM ELEMENT. PROJECT, TASK AREA & WORK UNIT NUMBERS
11. CONTROLLING OFFICE NAME AND ADDRESS Department of the Navy Office of Naval Research Arlington, VA 22217		12. REPORT DATE January 1995
		13. NUMBER OF PAGES 25 + Figs 1a-16b
14. MONITORING AGENCY NAME & ADDRESS(If different from Controlling Office)		15. SECURITY CLASS. (of this report)
		15a. DECLASSIFICATION/ DOWNGRADING SCHEDULE

16. DISTRIBUTION STATEMENT (of this Report)

Approved for public release: distribution unlimited

17. DISTRIBUTION STATEMENT (of the abstract entered in Block 20, if different from Report)

18. SUPPLEMENTARY NOTES

19. KEY WORDS (Continue on reverse side if necessary and identify by block number)

20. ABSTRACT

In [1] we showed that the error in the finite-element solution has two parts, namely, the local-error and the pollution-error and in [2] we gave methods for estimating and controlling the pollution-error in any region of interest. In this paper we will show that the control of the pollution-error is essential in order to guarantee that the derivatives obtained from local recoveries have higher accuracy than the derivatives computed directly from the finite-element solution and that this control must be more stringent than the one needed to guarantee the reliability of local a-posteriori error estimation. We give an algorithm for controlling the local and the pollution-error simultaneously, in any region of interest. We show that, when one is interested in obtaining high accuracy only in some parts of the domain, the proposed algorithm gives meshes which are much more economical than the ones obtained from the classical adaptive algorithms which control the global energy-norm of the error.

DD FORM 1473 1 JAN 73 EDITION OF 1 NOV 65 IS OBSOLETE

S N 0102-LF-014-6601

Pollution Error in the *h*-Version of the Finite Element Method and the Local Quality of the Recovered Derivatives

I. Babuška *

Institute for Physical Science and Technology and Department of Mathematics,
University of Maryland, College Park, MD 20742, U.S.A.

T. Strouboulis[†], S.K. Gangaraj[†] and C.S. Upadhyay[†]

Department of Aerospace Engineering, Texas A&M University,
College Station, TX 77843, U.S.A.

December 1994

1

Abstract:

In [1] we showed that the error in the finite-element solution has two parts, namely, the *local-error* and the *pollution-error* and in [2] we gave methods for estimating and controlling the pollution-error in any region of interest. In this paper we will show that the control of the pollution-error is essential in order to guarantee that the derivatives obtained from local recoveries have higher accuracy than the derivatives computed directly from the finite-element solution and that this control must be more stringent than the one needed to guarantee the reliability of local a-posteriori error estimation. We give an algorithm for controlling the local and the pollution-error simultaneously, in any region of interest. We show that, when one is interested in obtaining high accuracy only in some parts of the domain, the proposed algorithm gives meshes which are much more economical than the ones obtained from the classical adaptive algorithms which control the global energy-norm of the error.

1 Introduction

Let u_h be the finite element solution of the Laplacian in the domain Ω computed using a mesh T_h and let us assume that we are interested in the error $e_h = u - u_h$ in a mesh-patch $\omega^h \subset \Omega$, where u denotes the exact solution. In [1] we showed that

$$e_h\big|_{\omega^h} = V_1^{\tilde{\omega}^h} + V_2^{\tilde{\omega}^h} \tag{1.1}$$

where $V_1^{\tilde{\omega}^h}$ is the *local-error*, $V_2^{\tilde{\omega}^h}$ is the *pollution-error* and $\tilde{\omega}^h \subset \Omega$ consists of the mesh-patch ω^h together with a few surrounding mesh-layers. The precise definition of $V_i^{\tilde{\omega}^h}$, $i = 1, 2$ will be given in Section 2 below. The local-error $V_1^{\tilde{\omega}^h}$ is practically the error in the finite-element solution of the Laplacian in $\tilde{\omega}^h$ with Dirichlet boundary-conditions equal to u on the boundary of $\tilde{\omega}^h$. The pollution-error $V_2^{\tilde{\omega}^h}$ is practically the exact solution of the Laplacian with Dirichlet boundary-conditions equal to $(u - u_h)$ on the boundary of $\tilde{\omega}^h$.

We will now give an example which illustrates the above definitions. Let us consider the L-shaped domain shown in Fig. 1a with boundary-conditions corresponding to the exact solution $u(r, \vartheta) = r^{\frac{2}{3}} \sin\left(\dfrac{2\vartheta}{3}\right)$. We computed the finite-element solution using the uniform mesh of quadratic triangles shown in Fig. 1a. We let $\tilde{\omega}^h = (0.375, 0.625)^2$ and computed $V_1^{\tilde{\omega}^h}$, $V_2^{\tilde{\omega}^h}$ using the definitions given in Section 2. In Fig. 1b we give the graphs $\nabla V_1^{\tilde{\omega}^h} \cdot s$, $\nabla V_2^{\tilde{\omega}^h} \cdot s$, where s is the unit-vector along $A_1 A_3$. We note that the local-error $\nabla V_1^{\tilde{\omega}^h} \cdot s$ oscillates around zero whereas the pollution-error $\nabla V_1^{\tilde{\omega}^h} \cdot s$ is almost constant in ω^h.

Let $\tilde{\sigma}(W)$ denote a local-averaging applied to the vector-field W. For example, $\tilde{\sigma}(W)$ may be constructed by employing local least-squares smoothing as in the 'superconvergent patch-recovery' proposed in [3-4] (see Section 4, below). By the construction of $\tilde{\sigma}$, we have $\tilde{\sigma}(\alpha_1 W_1 + \alpha_2 W_2) = \alpha_1 \tilde{\sigma}(W_1) + \alpha_2 \tilde{\sigma}(W_2)$ and thus

$$\tilde{\sigma}(\nabla u_h) = \tilde{\sigma}(\nabla u) - \tilde{\sigma}(\nabla e_h) = \tilde{\sigma}(\nabla u) - \tilde{\sigma}(\nabla V_1^{\tilde{\omega}^h}) - \tilde{\sigma}(\nabla V_2^{\tilde{\omega}^h}) \tag{1.2}$$

Further, it can be shown that

$$\check{\sigma}(\nabla V_1^{\tilde{\omega}^h}) \approx 0, \qquad \check{\sigma}(\nabla V_2^{\tilde{\omega}^h}) \approx \nabla V_2^{\tilde{\omega}^h} \tag{1.3}$$

and hence

$$\tilde{\sigma}(\nabla u) - \tilde{\sigma}(\nabla u_h) \approx \nabla V_2^{\tilde{\omega}^h} \tag{1.4a}$$

From the asymptotic analysis

$$|\tilde{\sigma}(\nabla u) - \nabla u| << |\tilde{\sigma}(\nabla u) - \nabla u_h| \tag{1.4b}$$

3

and hence

$$\tilde{\sigma}(\nabla u) - \nabla u_h \approx \nabla e_h \qquad (1.4c)$$

which implies

$$\tilde{\sigma}(\nabla u_h) - \nabla u_h \approx \nabla V_1^{\tilde{\omega}^h} \qquad (1.4d)$$

For example, from Fig. 1b we can see that

$$\left(\tilde{\sigma}(\nabla u_h) - \nabla u_h\right) \cdot s \approx \nabla V_1^{\tilde{\omega}^h} \cdot s \ .$$

Thus, $\tilde{e}_\sigma = \tilde{\sigma}(\nabla u_h) - \nabla u_h$, which is often used as an error-indicator, *estimates only the local-error*, namely $\tilde{e}_\sigma \approx \nabla V_1^{\tilde{\omega}^h}$.

In [5] we have shown that

$$\left|\tilde{\sigma}(\nabla u) - \nabla u\,\right|(\bar{x}) \le 0.20 \max_{x \in \tau} |\nabla V_1^{\tilde{\omega}^h}|(\bar{x}), \qquad \bar{x} \in \tau \subseteq \omega^h \qquad (1.5)$$

where 0.20 is an empirical constant which was estimated from the numerical results in [5] (these results were obtained for large classes of grids of triangles and quadrilaterals). Eq. (1.5) was established under conditions which guarantee that the pollution error vanishes identically, i.e. $\nabla V_2^{\tilde{\omega}^h} \equiv 0$. In general, we have

$$\tilde{\sigma}(\nabla u_h) - \nabla u \approx \tilde{\sigma}(\nabla u) - \nabla u - \nabla V_2^{\tilde{\omega}^h} \qquad (1.6)$$

and thus

$$|\tilde{\sigma}(\nabla u_h) - \nabla u|(\bar{x}) \le |\tilde{\sigma}(\nabla u) - \nabla u|(\bar{x}) + |\nabla V_2^{\tilde{\omega}^h}|(\bar{x})$$

$$(1.7)$$

$$\le 0.20 \max_{x \in \tau} |\nabla V_1^{\tilde{\omega}^h}|(x) + \max_{x \in \tau} |\nabla V_2^{\tilde{\omega}^h}|(x)$$

for any $\bar{x} \in \tau \subseteq \omega^h$. Hence, in order to control the error in the recovered-gradient we must control $\max_{x \in \tau} |\nabla V_2^{\tilde{\omega}^h}|(x)$ relative to $0.20 \max_{x \in \tau} |\nabla V_1^{\tilde{\omega}^h}|(x)$. Thus we must design the mesh such that

$$\max_{x \in \tau} |\nabla V_2^{\tilde{\omega}^h}|(x) \le s^{\%} \left(0.20 \max_{x \in \tau} |\nabla V_1^{\tilde{\omega}^h}|(x)\right) \qquad (1.8)$$

for some tolerance $s^{\%} \le 100\%$. In the numerical examples we will show that, in general, if (1.8) is not enforced by proper design of the mesh the accuracy of the recovered-derivatives is practically the same as the accuracy of the derivatives computed directly from the finite-element solution.

The goals of this paper are:

1. To show that, in practical computations, the pollution-error can be large relative to the local-error, in regions of interest, and, if this is the case, there is no gain in the accuracy from local recoveries.

2. To construct adaptive methods which guarantee the accuracy of the recovered-derivatives in a region of interest.

Remark 1.1. In [2] we showed that in order to obtain reliable error-estimators for the energy-norm in a patch of elements one must control the magnitude of the pollution-error relative to the local-error in the patch. Here we show that in order to guarantee that the derivatives, computed using a local recovery, are of higher pointwise accuracy than the derivatives computed directly from the finite-element solution one needs to employ more stringent control of the pollution than the control needed to ensure the local quality of the energy error-estimators over a mesh-patch.

Following this Introduction we give notations related to the model problem and define the pollution-error and its a-posteriori estimate. We give an algorithm for the adaptive control of the pollution-error relative to the local-error in any region of interest. We then give numerical examples which demonstrate that the recovered derivatives have higher accuracy than the derivatives computed directly from the finite-element solution only if the pollution-error is controlled relative to the local-error.

2   Definition and a-posteriori estimation of the pollution-error

Let $\Omega \subseteq \mathbf{R}^2$ denote a polygonal domain with boundary $\partial\Omega = \Gamma = \bar{\Gamma}_D \cup \Gamma_N$ where Γ_D is the Dirichlet and Γ_N is the Neumann-boundary and $\bar{\Gamma}_D \cap \Gamma_N = \emptyset$. We will consider the mixed boundary-value problem for the Laplacian which, in variational form, reads:

Find $u \in H^1_{\Gamma_D} := \left\{ u \in H^1(\Omega) \, \middle| \, u = 0 \text{ on } \Gamma_D \right\}$ such that

$$B_\Omega(u, v) := \int_\Omega \nabla u \cdot \nabla v = \int_{\Gamma_N} f v \qquad \forall \, v \in H^1_{\Gamma_D} \tag{2.1}$$

If $\Gamma_D = \emptyset$, it is assumed that f satisfies the consistency condition $\int_\Gamma f = 0$. In this case the solution u is determined uniquely up to an arbitrary constant.

For the finite element method we partition the domain Ω into square (or quadrilateral) elements with straight edges τ defined by the mesh T_h and let

$$S^p_h(\Omega) := \left\{ v_h \in H^1_{\Gamma_D}(\Omega) \, \middle| \, v_h|_\tau \in S^p_h(\tau) \quad \forall \, \tau \in T_h \right\} \tag{2.2}$$

(For the quadrilateral elements we employ the bilinear mapping to define the shape-functions over a given element.) Here $S_h^p(\tau)$ denotes the *finite-element space* over τ and p is the degree of the elements. We employed the *biquadratic polynomial space* $(p = 2)$

$$S_h^2(\hat{\tau}) := \left\{ P \ \Big| \ P(x_1, x_2) = \sum_{\substack{i,j \\ 0 \le i,j \le 2}} \alpha_{i,j} \, x_1^i \, x_2^j \right\} \tag{2.3}$$

The finite element approximation of the solution of (2.1) satisfies:

Find $u_h \in S_{h,\Gamma_D}^p := S_h^p(\Omega) \cap H_{\Gamma_D}^1(\Omega)$ such that

$$B_\Omega(u_h, v_h) = \int_{\Gamma_N} f \, v_h \qquad \forall \ v_h \in S_{h,\Gamma_D}^p \tag{2.4}$$

Let ε be an edge and J_ε denote the *jump of the normal derivative of u_h on ε*, defined by:

$$J_\varepsilon := \begin{cases} \left(\nabla u_h \big|_{\tau_{in}} - \nabla u_h \big|_{\tau_{out}} \right) \cdot \boldsymbol{n}_\varepsilon, & \varepsilon \not\subseteq \partial\Omega \\[3mm] 2\left(f - \nabla u_h \big|_{\tau_{out}} \right) \cdot \boldsymbol{n}_\varepsilon, & \varepsilon \subseteq \Gamma_N \\[3mm] 0, & \varepsilon \subseteq \Gamma_D \end{cases} \tag{2.5}$$

Here $\boldsymbol{n}_\varepsilon$, τ_{in} and τ_{out} denote the unit-normal and the elements associated with the edge ε, as shown in Fig. 2. The error $e_h := u - u_h$ satisfies the *residual-equation*:

Find $e_h \in H_{\Gamma_D}^1$ such that

$$B_\Omega(e_h, v) = \sum_{\tau \in T_h} \mathcal{F}_\tau(v) \qquad \forall \ v \in H_{\Gamma_D}^1 \tag{2.6}$$

where $\mathcal{F}_\tau$ denotes the element-residual functional given by

$$\mathcal{F}_\tau(v) := \int_\tau v \Delta u_h \Big|_\tau + \frac{1}{2} \sum_{\epsilon \subseteq \partial\tau} \int_\epsilon v J_\epsilon \ , \qquad v \in H_{\Gamma_D}^1 \tag{2.7}$$

Let us assume that the element-residuals have been modified in the following way (for the construction see [2] and [7]; see also [8-9])

$$\mathcal{F}_\tau^{EQ}(v) := \mathcal{F}_\tau(v) + \sum_{\varepsilon \subseteq \partial\tau \cap E_{int}} \int_\varepsilon v \theta_\tau^\varepsilon \tag{2.8}$$

such that

6

$$\mathcal{F}_\tau^{EQ}(v) = 0 \qquad \forall \ v \in S_h^p(\tau) \tag{2.9}$$

Here θ_τ^ε is the *correction* for the edge ε and the element τ and E_{int} is the set of interior edges. For any interior edge ε it is assumed that $\theta_{\tau_{in}}^\varepsilon = -\theta_{\tau_{out}}^\varepsilon$. We then have

$$B_\Omega(e_h, v) = \sum_{\tau \in T_h} \mathcal{F}_\tau^{EQ}(v) \qquad \forall \ v \in H_{\Gamma_D}^1 \tag{2.10}$$

Let ω^h be a patch of elements and let $\tilde{\omega}^h$ denote a patch which consists of ω^h and a few mesh-layers around it (in the results below $\tilde{\omega}^h$ consists of ω^h and two mesh-layers around it). Let $V_1^{\tilde{\omega}^h} \in H_{\Gamma_D}^1$ be the *local-error* in ω^h defined by

$$B_\Omega(V_1^{\tilde{\omega}^h}, v) = \sum_{\substack{\tau \in T_h \\ \tau \subseteq \tilde{\omega}^h}} \mathcal{F}_\tau^{EQ}(v) \qquad \forall \ v \in H_{\Gamma_D}^1 \tag{2.11}$$

Then the *pollution-error* in ω^h is $V_2^{\tilde{\omega}^h} := e_h - V_1^{\tilde{\omega}^h}$. In [2] we have proven that

$$\frac{\partial V_2^{\tilde{\omega}^h}}{\partial x_i}(\bar{x}) = \sum_{\substack{\tau \in T_h \\ \tau \not\subseteq \tilde{\omega}^h}} B_\tau(\hat{e}_\tau, G_i^{(\bar{x})} - w_\tau) \tag{2.12}$$

where w_τ is the best-approximation of $G_i^{(\bar{x})}$ in τ by biquadratic polynomials and $G_i^{(\bar{x})}$, $\bar{x} \in \Omega$ is the function which satisfies

$$-\Delta G_i^{(\bar{x})} = -\frac{\partial \delta}{\partial x_i}(\bar{x}) \qquad \text{in} \quad \Omega \tag{2.13a}$$

$$G_i^{(\bar{x})} = 0 \qquad \text{on} \quad \Gamma_D \tag{2.13b}$$

$$\frac{\partial}{\partial n} G_i^{(\bar{x})} = 0 \qquad \text{on} \quad \Gamma_N \tag{2.13c}$$

Here $i = 1$ or 2 and $\dfrac{\partial \delta}{\partial x_i}(\bar{x})$ denotes the x_i-derivative of Dirac's delta centered at $\bar{x}$. Eq. (2.13a) is understood in the sense of the theory of distributions.

An a-posteriori estimate of $\left| \dfrac{\partial V_2^{\omega^h}}{\partial x_i}(\bar{x}) \right|$, based on (2.12), can be constructed by employing the following steps. Assuming that $\bar{x}$ is a nodal point of the mesh, we compute the finite element approximation $\tilde{G}_{i,h}^{(\bar{x})} \in S_{h,\Gamma_D}^p$ of the solution of (2.13) by solving

$$B_\Omega(\tilde{G}_{i,h}^{(\bar{x})}, v) = \frac{1}{h}\Big(v(\bar{x} + n_i h) - v(\bar{x})\Big) \qquad \forall \ v \in S_{h,\Gamma_D}^p \qquad (2.14a)$$

when n_i is the unit-vector in the i-th direction. We assume that $\bar{x} + n_i h$ is also a nodal point of the mesh (this can be always achieved with obvious modifications of the approximation of $G_i^{(\bar{x})}$). The function $\tilde{G}_{i,h}^{(\bar{x})}$ is the finite-element approximation of

$$\tilde{G}_i^{(\bar{x})}(\tilde{x}) := \frac{1}{h}\Big(G^{(\bar{x}+hn_i)}(\tilde{x}) - G^{(\bar{x})}(\tilde{x})\Big) \qquad (2.14b)$$

where $G^{(\bar{x})}$ is the classical Green's function which satisfies (2.13) with the right-hand side of (2.13a) replaced by $\delta(\bar{x})$. Then, we get (see [2])

$$\left|\frac{\partial V_2^{\tilde{\omega}^h}}{\partial x_i}(\bar{x})\right| \le \bigg(\sum_{\substack{\tau \in T_h \\ \tau \not\subseteq \tilde{\omega}^h}} |B_\tau(\hat{e}_\tau, \tilde{G}_{i,h}^{(\bar{x})} - \tilde{w}_\tau)|\bigg)(1 + \mathcal{C}h) \qquad (2.14c)$$

where $\tilde{w}_\tau$ is the best-approximation of $\tilde{G}_i^{(\bar{x})}$ by quadratic polynomials in τ.

We define the *pollution-indicators for the i-th derivative*

$$\mu_{i,\tau}^{(1)}(\bar{x}) := \Big|B_\tau\Big(\hat{e}_\tau(u_h), \hat{e}_\tau(\tilde{G}_{i,h}^{(\bar{x})})\Big)\Big| \qquad (2.15a)$$

$$\mu_{i,\tau}^{(2)}(\bar{x}) := \|\nabla\hat{e}_\tau(u_h)\|_\tau \, \|\nabla\hat{e}_\tau(\tilde{G}_{i,h}^{(\bar{x})})\|_\tau = \eta_\tau(u_h)\eta_\tau(G_{i,h}^{(\bar{x})}) \qquad (2.15b)$$

where $\hat{e}_\tau(u_h)$ and $\hat{e}_\tau(\tilde{G}_{i,h}^{(\bar{x})})$ $\big($resp. $\eta_\tau(u_h)$ and $\eta_\tau(\tilde{G}_{i,h}^{(\bar{x})})\big)$ are the error-indicator functions (resp. element error-indicators) corresponding to u_h and $\tilde{G}_{i,h}^{(\bar{x})}$, respectively. We then define the *pollution-estimate for the i-th derivative in ω^h*

$$\mathcal{M}_i^{(k)}(\bar{x}) = \sum_{\substack{\tau \in T_h \\ \tau \not\subseteq \tilde{\omega}^h}} \mu_{i,\tau}^{(k)}(\bar{x}), \qquad i = 1, 2, \qquad k = 1, 2 \qquad (2.15c)$$

The above quantities can be computed by employing the error-indicator functions obtained from the local problems:

Find $\hat{e}_\tau \in \overset{0}{H}{}^1(\tau)$ such that

$$B_\tau(\hat{e}_\tau, v) = \mathcal{F}_\tau^{EQ}(v) \qquad \forall \ v \in \overset{0}{H}{}^1(\tau) \qquad (2.16a)$$

where

$$\overset{0}{H}{}^1(\tau) = \Big\{ v \in H^1\Big|_\tau \quad v\Big|_{\partial\tau \cap \Gamma_D} = 0 \Big\} \qquad (2.16b)$$

8

In the computations we approximate $\hat{e}_\tau$ using biquartic polynomials. The function $\hat{e}_\tau(u_h)$ $\left(\text{resp. } \hat{e}_\tau(\tilde{G}^{(x)}_{i,h})\right)$ is the exact solution of (2.16) for the residual $\mathcal{F}^{EQ}_\tau$ corresponding to u_h (resp. $G^{(x)}_{i,h}$). In [2] we have shown that

$$\left|\frac{\partial V_2^{\tilde{\omega}^h}}{\partial x_i}\right| \leq \mathcal{M}^{(2)}_i(\bar{x})(1 + \mathcal{C}h) \tag{2.17}$$

provided that the element error-indicators are accurate, modulo the pollution-error. From the numerical studies given in [2] we have seen that $\mathcal{M}^{(1)}_i(\bar{x})$ has essentially the same properties as $\mathcal{M}^{(2)}_i(\bar{x})$.

Remark 2.1. In [2] we showed that the above a-posteriori estimates of the pollution give effectivity indices $\dfrac{\mathcal{M}^{(k)}_i(\bar{x})}{\left|\dfrac{\partial V_2^{\omega^h}}{\partial x_i}(\bar{x})\right|}$, $k = 1, 2$ close to one. In the numerical studies given below we employed only $\mathcal{M}^{(1)}_i$ (in the discussion below the exponent will be omitted).

Remark 2.2. For a complete discussion of the underlying mathematical framework for the pollution problem see [6].

3   Adaptive algorithms

We will now give two adaptive algorithms which can be employed to control the local accuracy of the solution. The first is the classical feedback-algorithm for the control of the global energy-norm (e.g. [10]; see also [11] and [12] for a different approach) while the second is a new feedback-algorithm for the simultaneous control of the local and the pollution-error only in a mesh-patch ω^h.

3.1   Globally-adaptive grid

Let $t\%$ be a given tolerance and let us assume that the goal is to construct a mesh for which

$$||\nabla e_h||_\Omega \leq t\%||\nabla u||_\Omega \tag{3.1}$$

where $||W||^2_\Omega = \int_\Omega W \cdot W$.

We will construct such a mesh by employing the following algorithm:

1. Let $T_h \equiv T^0_h$ and go to 3.

2. For each element $\tau \in T_h$ do:

9

2.1. Compute $\eta_\tau := ||\nabla \hat{e}_\tau||_\tau$

2.2. If $\eta_\tau \geq \gamma \, \underset{\tau}{max} \, \eta_\tau$, subdivide τ.

3. Compute the finite element solution on T_h and $\mathcal{E}_\Omega = \sqrt{\sum_{\tau \in T_h} \eta_\tau^2}$.

4. Check if

$$\mathcal{E}_\Omega \leq t\% ||\nabla u_h||_\Omega$$

If not go to 2, otherwise stop.

Here T_h^0 is the initial mesh, η_τ denotes the *element error-indicator*, $\mathcal{E}_\Omega$ is an estimate for $||\nabla e_h||_\Omega$ and $0 < \gamma < 1$ is a parameter. In the computations below, we took $\gamma = 0.9$.

Remark 3.1. It should be noted that the above algorithm does not allow for the direct control of the local accuracy in a region of interest. The local accuracy can be controlled indirectly through the value of the tolerance for the global energy-norm.

Remark 3.2. The above algorithm produces meshes which are *nearly-equilibrated* in the energy-norm. In [1] we showed that, for nearly-equilibrated meshes, the pollution-error is (indirectly) controlled relative to the local-error.

Remark 3.3. We underline that the constructed meshes are dependent on T_h^0 which reflects the domain of interest (i.e. the domain of interest should coincide exactly with one element or the union of several elements from the coarsest mesh).

3.2 Global/local adaptive grid

Let us assume that the goal of the computation is to achieve a prescribed $t\%$-accuracy in the relative-error for the recovered-gradient in the mesh-patch ω^h, namely

$$\frac{|\tilde{\sigma}(\nabla u_h) - \nabla u|(x)}{\bar{\sigma}_{\omega^h}} \leq t\%, \qquad x \in \omega^h \tag{3.2}$$

where $\bar{\sigma}_{\omega^h}^2$ is an average-value of the square of the gradient of the exact-solution over ω^h,

$$\bar{\sigma}_{\omega^h} = \frac{1}{\sqrt{|\omega^h|}} \sqrt{\int\!\!\int_{\omega^h} |\nabla u|^2} \tag{3.3}$$

From (1.7) we see that this goal can be achieved by designing the grid such that

$$\xi_{\omega^h} := \frac{\|\nabla V_1^{\tilde{\omega}^h}\|_{\omega^h}}{\bar{\sigma}_{\omega^h}} \approx p\% \tag{3.4}$$

and then enforcing the condition

$$\|\nabla V_2^{\tilde{\omega}^h}\|_{\omega^h} \le \delta\% \|\nabla V_1^{\tilde{\omega}^h}\|_{\omega^h} \tag{3.5}$$

Remark 3.4. Note that (3.4) and (3.5) were obtained from (1.7) and (1.8), respectively by replacing the maximum norm by the average mean-square value i.e. by assuming that

$$\max_{x \in \tau} |\nabla V_i^{\tilde{\omega}^h}| \approx \mathcal{C} \, \frac{\|\nabla V_i^{\tilde{\omega}^h}\|_{\omega^h}}{\sqrt{|\omega^h|}} \tag{3.6}$$

The grid which controls, simultaneously, the local- and the pollution-error in ω^h is constructed using the following algorithm:

1. Let $T_h \equiv T_h^0$ and set flag $= 0$.

2. Compute the finite element solution on T_h.

3. Check if

$$\xi_{\omega^h} \le t\% \tag{3.7}$$

   If yes and flag $= 0$ go to step 5.
   If yes and flag $= 1$ go to step 7.

4. For each element $\tau \in T_h$:

   4.1 Compute $\tilde{\eta}_\tau := \|\nabla \hat{e}_\tau\|_\tau$
   4.2 If $\tilde{\eta}_\tau \ge \gamma \max\limits_{\substack{\tau \in T_h \\ \tau \subseteq \omega_0}} \tilde{\eta}_\tau$, subdivide τ.
   Set flag $= 0$ and go to step 2.

5. Compute the *pollution-estimate for the gradient*

$$\mathcal{M}_{\omega^h} = \sqrt{|\omega^h|} \sqrt{\sum_{\substack{\tau \in T_h \\ \tau \not\subseteq \tilde{\omega}_0}} (\mu_{1,\tau}^2 + \mu_{2,\tau}^2)} \tag{3.8}$$

   Check if

11

$$\mathcal{M}_{\omega^h} \leq \delta\% \, \mathcal{E}_{\omega^h} \qquad\qquad (3.9)$$

If yes set flag $= 1$ and go to step 2.

6. For each element $\tau \in T_h$, $\tau \not\subseteq \tilde{\omega}^h$:

    6.1 Compute the pollution-indicator for the gradient in τ, $\mu_\tau = \sqrt{\mu_{1,\tau}^2 + \mu_{2,\tau}^2}$.

    6.2 If $\mu_\tau \geq \bar{\gamma} \max\limits_{\substack{\tau \in T_h \\ \tau \not\subseteq \tilde{\omega}^h}} \mu_\tau$, subdivide τ.

    Compute the finite element solution on the new mesh and go to step 5.

7. Stop.

In the numerical examples below we employed $\bar{\gamma} = 0.9$. The grid constructed as described above will be called *global/local adaptive grid* with respect to ω^h.

Remark 3.5. Note that the above algorithm gives us direct control of the accuracy of the finite element solution in the mesh-patch ω^h.

Remark 3.6. The global/local adaptive meshes are obtained by enforcing, simultaneously, (3.7) and (3.9).

Remark 3.7. The meshes constructed by the feedback algorithm in steps 4, 5 are called *pollution-adaptive* with respect to ω^h.

Remark 3.8. We underline that, for the global/local adaptive grids, the error in the mesh-patch of interest may be controlled to be as small as desired while, at the same time, the error in the global energy-norm may be very large.

Remark 3.9. A different approach for constructing global/local adaptive grids is given in [13].

4   The quality of the recovered derivatives in the interior of the mesh

Practical computations involve polygonal domains with several reentrant corners and points where the type of boundary-conditions changes from Dirichlet to Neumann. In such computations the effect of the pollution can be very significant. Let us consider a boundary-value problem with two-singular points as our model example. Let Ω be the polygonal domain ABCDEFGH shown in Fig. 3 and let the exact solution

$$u(x_1, x_2) = r_C^{\frac{1}{3}} \sin\left(\frac{\vartheta_C}{3}\right) + r_F^{\frac{2}{3}} \sin\left(\frac{2\vartheta_F}{3}\right)$$

where $r_C = \sqrt{(x_1 - (x_C)_1)^2 + (x_2 - (x_C)_2)^2}$ and similarly for r_F, while ϑ_C (resp. ϑ_F) is the angle measured in the clockwise (resp. counter-clockwise) direction from BC (resp. FG). We let $A = (-1,1)$, $B = (-1,0)$, $C = (0,0)$, $D = (0,-1)$, $E = (2,-1)$, $F = (2,0)$, $G = (3,0)$, $H = (3,1)$. We considered the mesh-patches ω_1^h and ω_2^h which consist of the part of the mesh which covers the fixed subdomains $\Omega_1 = (0.375, 0.625) \times (-0.625, -0.375)$ and $\Omega_2 = (2.375, 2.625) \times (0.375, 0.625)$, respectively. (In the examples below we will use an initial mesh T_h^0 which includes elements which cover exactly Ω_1 and Ω_2. This mesh is different than the initial mesh employed to arrive to the uniform mesh depicted in Fig. 3.) The goal of the computations given below, is *to control the accuracy of the finite-element solution* (in the subdomains Ω_1 and Ω_2) *below a given tolerance and, at the same time, to obtain better accuracy, than the accuracy achieved by the finite-element solution* (in these subdomains), *by employing the recovered derivatives.*

In the numerical results below we will utilize the following quantities to report the accuracy achieved by the gradient of the finite-element solution and the recovered-gradient in a mesh-patch ω^h.

1. *The pointwise and the maximum relative-error in the gradient of the finite-element solution in ω^h:*

$$\rho_h(x) = \frac{|\nabla u - \nabla u_h|(x)}{\bar{\sigma}_{\omega^h}}, \qquad \rho_{\omega^h} = \max_{x \in \omega^h} \rho_h(x) \qquad (4.1)$$

2. *The pointwise and the maximum relative-error in the recovered-gradient in ω^h:*

$$\pi_h(x) = \frac{|\nabla u - \tilde{\sigma}(\nabla u_h)|}{\bar{\sigma}_{\omega^h}}, \qquad \pi_{\omega^h} = \max_{x \in \omega^h} \pi_h(x) \qquad (4.2)$$

3. *The pointwise effectivity-index for the error-estimator based on the recovered-gradient in ω^h:*

$$\kappa(x) = \frac{|\tilde{\sigma}(\nabla u_h) - \nabla u_h|(x)}{|\nabla u - \nabla u_h|(x)} \qquad (4.3)$$

In the numerical examples below, we employed the 'superconvergent patch-recovery' (given in [3-5]) to construct the recovered derivatives $\tilde{\sigma}(\nabla u_h)$. In particular, for the biquadratic elements employed in the examples we let:

$$\tilde{\sigma}(\nabla u_h)\big|_\tau = \sum_X \sigma^*_X(\nabla u_h)\big|_X N_X + \sum_Y \frac{1}{2}\Big(\sigma^*_{X_1}(\nabla u_h)\big|_Y + \sigma^*_{X_2}(\nabla u_h)\big|_Y\Big)N_Y$$

$$\tag{4.4}$$

$$+ \frac{1}{4}\Big(\sigma^*_{X_1}(\nabla u_h)\big|_Z + \sigma^*_{X_2}(\nabla u_h)\big|_Z + \sigma^*_{X_3}(\nabla u_h)\big|_Z + \sigma^*_{X_4}(\nabla u_h)\big|_Z\Big)N_Z$$

where X, Y, Z denote a vertex, mid-side node and the centroid of the quadrilateral element τ and $\sigma^*_X(\nabla u_h)$ is computed as the solution of the following minimization problem over the patch of elements connected to the vertex X:

Find $\sigma^*_X(\nabla u_h) \in \mathcal{P}_2$ such that

$$\sum_{\ell=1}^{nsamp} (\sigma^*_X(\nabla u_h) - \nabla u_h)^2(x_\ell) \leq \sum_{\ell=1}^{nsamp} (\sigma - \nabla u_h)^2(x_\ell) \qquad \forall\ \sigma \in \mathcal{P}_2 \tag{4.5}$$

Here $\{x_\ell\}_{\ell=1}^{nsamp}$ are the sampling-points which are taken to be the mapped (2×2) Gauss-Legendre points in the quadrilaterals connected to the vertex X. For the details about the implementation see [3-5].

4.1 The quality of the recovered derivatives in uniform grids

First, let us assume that we would like to employ a uniform mesh of biquadratic elements. (Note that many practical computations are performed using quasi-uniform meshes of elements of quadratic degree.) We employed uniform meshes of mesh-size $h = \dfrac{1}{8}$ and $\dfrac{1}{16}$ with total number of degrees of freedom 1633 and 6337, respectively. For the uniform-mesh with $h = \dfrac{1}{8}$ we obtained

$$\rho_{\omega_1^h} = 34.62\%, \qquad \pi_{\omega_1^h} = 36.09\%$$

$$\rho_{\omega_2^h} = 19.38\%, \qquad \pi_{\omega_2^h} = 16.47\%$$

and for the uniform-mesh with $h = \dfrac{1}{16}$

$$\rho_{\omega_1^h} = 16.39\%, \qquad \pi_{\omega_1^h} = 16.67\%$$

$$\rho_{\omega_2^h} = 12.30\%, \qquad \pi_{\omega_2^h} = 11.79\%$$

We observe the following:

14

1. Even for the relatively refined mesh with $h = \dfrac{1}{16}$ we cannot obtain 5% accuracy in the recovered-gradient in any of the subdomains.

2. The error in the recovered derivatives is practically the same as the error in the derivatives of the finite-element solution in both subdomains.

3. The pointwise effectivity index for the estimator based on recovered derivatives in the interior of the subdomains is practically equal to zero.

4.2 The quality of the recovered derivatives for grids refined only in a subdomain of interest

An approach which is often used in engineering analysis of complex structures is to refine the mesh locally only in regions of interest (see for example [14-16]). To show that this approach is meaningless, in general, let us refine the mesh in the neighborhood of subdomain Ω_1 as shown in Fig. 4 $\left(\text{the local uniform mesh-size in}\right.$ Ω_1 is equal to $\dfrac{1}{64}$$\left.\right)$. Using this mesh we obtained for $\omega_1^h \equiv \left\{ \tau \in T_h \mid \tau \subseteq \Omega_1 \right\}$

$$\rho_{\omega_1^h} = 84.53\%, \qquad \pi_{\omega_1^h} = 96.17\%$$

while the estimated relative-error was

$$\frac{\mathcal{E}_{\omega_1^h}}{\|\nabla u\|_{\omega_1^h}} = 0.00036\%$$

The above results can be explained as follows: As we have already discussed in the Introduction we have

$$\tilde{\sigma}(\nabla u_h) - \tilde{\sigma}(\nabla u) \approx \nabla V_2^{\tilde{\omega}^h}$$

Since we are refining the mesh only inside Ω_1 the gradient of the pollution-error $\nabla V_2^{\tilde{\omega}^h}$ is practically constant in the interior of the subdomain and hence, in general, we cannot increase the accuracy of the recovered derivatives by refining the mesh, locally, only in the subdomain $\tilde{\omega}^h$. Further, we have

$$\tilde{\sigma}(\nabla u_h) - \nabla u_h \approx \nabla V_1^{\tilde{\omega}^h}$$

and thus, as the subdomain is refined, the estimated error converges to zero while the true error remains practically constant. For additional results and a complete discussion of the performance of estimators in the interior of locally refined meshes see [6].

4.3 The quality of the recovered derivatives for globally-adaptive grids

In [6] we showed that when the mesh is nearly-equilibrated in the energy-norm (i.e. globally-adaptive) the pollution-error is controlled relative to the local-error and the element error-indicators have effectivity-indices close to one everywhere in the mesh. *Here we would like to demonstrate that the quality of the derivatives computed by local-recoveries is more sensitive to the pollution-error, than the quality of the local element error-indicators.*

We employed the feedback algorithm with $\gamma = 0.9$ and constructed a sequence of adaptive grids. The convergence of the global energy-norm versus the number of degrees of freedom for this sequence is given in Fig. 5d. We see that the rate of convergence for the sequence of adaptively-constructed meshes is $N^{\frac{p}{2}}$, where N is the number of degrees of freedom and p is the degree of the elements ($p = 2$). In Figs. 6a-6g we show seven meshes from the sequence of grids. These grids correspond to point T_1 through T_7 in the graph of Fig. 5. In Fig. 6d (resp. Fig. 6e) we give the globally-adaptive grid T_4 (resp. T_5) which achieves tolerance 4.77% (resp. 0.93%) in the global energy-norm. For the mesh T_4 (resp. T_5) we have $\rho_{\omega_1^h} = 28.2\%$, $\pi_{\omega_1^h} = 22.4\%$ (resp. $\rho_{\omega_1^h} = 8.48\%$, $\pi_{\omega_1^h} = 2.73\%$). In Fig. 7a (resp. Fig. 7b) we give the regions of 2.5%, 5% and 10% relative-error (shown dark-gray, gray, light-gray, respectively) for the gradient of the finite element solution (resp. the recovered gradient) in the subdomain ω_1^h, for the globally-adaptive mesh T_4 shown in Fig. 6d. Note that there is significant gain in the 10%-regions for the recovered gradient compared with the gradient computed directly from the finite-element solution. In Fig. 8a (resp. Fig. 8b) we give the regions of 0.5%, 1% and 2% relative-error in the gradient of the finite element solution (resp. the recovered gradient) in the subdomain ω_1^h for the globally-adaptive mesh T_5 shown in Fig. 6e. Note that there is a significant gain in the 2% regions for the recovered gradient compared with the gradient computed directly from the finite-element solution. In Fig. 9 we give the regions of 1%, 2%, 4% relative-error in the recovered gradient in the subdomain ω_2^h for the globally-adaptive mesh T_4. These regions will be compared with the regions given in the next Section for a global/local adaptive grid with respect to ω_2^h.

The above results can be explained as follows: By employing a mesh which is nearly-equilibrated in the energy-norm we are (indirectly) controlling the ratio

$$\frac{\max\limits_{x \in \tau} |\nabla V_2^{\tilde{\omega}^h}|(x)}{\max\limits_{x \in \tau} |\nabla V_1^{\tilde{\omega}^h}|(x)} \leq C$$

where τ is any element and $\tilde{\omega}^h$ is a mesh-patch which consists of τ and a few mesh-layers around it. Hence, from (1.7) we get

$$\left| \tilde{\sigma}(\nabla u_h) - \nabla u \right| (\bar{x}) \leq (0.20 + \mathcal{C}) \max_{x \in \tau} |\nabla V_1^{\tilde{\omega}^h}|(x), \qquad \bar{x} \in \tau$$

Thus if $\mathcal{C}$ is small we see that the error in the recovered gradient is less than the local error. Nevertheless, the accuracy of the recovered gradient may not be as high as predicted by the analysis in [1] because $\mathcal{C}$ may be comparable to 0.20.

In summary, we observe the following:

1. When a globally-adaptive grid is employed, with sufficiently small tolerance for the global energy-norm, the local accuracy of the recovered gradient is better than the local accuracy of the finite-element solution.

2. Depending on the data and the subdomain of interest, it may be very expensive to employ a globally adaptive grid to achieve high local accuracy in a subdomain.

4.4 The quality of the recovered derivatives in global/local adaptive grids

We now describe numerical studies on the quality of recovered derivatives in global/local adaptive grids which are obtained using the algorithm described in Section 3.2. Here we will show that:

(i) In general, we can obtain better accuracy in the recovered derivatives with fewer degrees of freedom, by employing a global/local adaptive grid with respect to the mesh-patch of interest instead of a globally-adaptive grid.

(ii) The quality of the recovered derivatives, computed from a global/local adaptive grid, can be enhanced by controlling the pollution-error to a sufficiently small tolerance.

We used the global/local adaptive algorithm on an initial mesh which has $h = \dfrac{1}{8}$ in ω_1^h and $h = 1$ in the rest of the domain. In Fig. 5 we give the convergence of the global energy-norm versus the number of degrees of freedom for the sequence of pollution-adaptive meshes with respect to the mesh-patch ω_1^h. We see that for the global/local adaptive mesh-sequence the error, measured in the global energy-norm, is practically constant i.e. it does not decrease with the refinement of the mesh. This sequence was obtained by fixing the mesh in ω_1^h and by using the feedback algorithm which employs the pollution-indicators to refine the mesh outside $\tilde{\omega}_1^h$. In Fig. 10a we show the mesh from the sequence which achieves $\dfrac{\mathcal{E}_{\omega_1^h}}{||\nabla u_h||_{\omega_1^h}} = 9.18\%$

17

and $\dfrac{\mathcal{M}_{\omega_1^h}}{\mathcal{E}_{\omega_1^h}} = 19.13\%$. For this mesh, which has 1053 degrees of freedom, $\rho_{\omega_1^h} = 29.95\%$, $\pi_{\omega_1^h} = 10.32\%$. In Fig. 10b we show the regions of the relative-error in the gradient of the finite element solution (i.e. ρ_h) and in Fig. 10c we show the regions of relative-error in the recovered gradient (i.e. π_h) in the subdomain ω_1^h, shown shaded in Fig. 10a. By comparing Figs. 10b and 10c, we observe that there is a significant gain in the 10%-relative-error regions when the recovered gradient is used instead of the gradient computed directly from the finite-element solution. We have, as before,

$$
|\tilde{\sigma}(\nabla u_h) - \nabla u|\,(\bar{x}) \le \left(0.20 + \frac{\max\limits_{x \in \tau} |\nabla V_2^{\tilde{\omega}_1^h}|(x)}{\max\limits_{x \in \tau} |\nabla V_1^{\tilde{\omega}_h}|(x)} \right) \max\limits_{x \in \tau} |\nabla V_1^{\tilde{\omega}_h}|(x), \qquad \bar{x} \in \tau \subseteq \omega_1^h
$$

and since

$$
\frac{\max\limits_{x \in \tau} |\nabla V_2^{\tilde{\omega}_1^h}|(x)}{\max\limits_{x \in \tau} |\nabla V_1^{\tilde{\omega}_1^h}|(x)} \approx \frac{\|\nabla V_2^{\tilde{\omega}_1^h}\|_{\omega_1^h}}{\|\nabla V_1^{\tilde{\omega}_1^h}\|_{\omega_1^h}} \approx \frac{\mathcal{M}_{\omega_1^h}}{\mathcal{E}_{\omega_1^h}}
$$

by choosing the mesh such that $\dfrac{\mathcal{M}_{\omega_1^h}}{\mathcal{E}_{\omega_1^h}} < 20\%$ we have ensured higher-order accuracy of $\tilde{\sigma}(\nabla u_h)$ in ω_1^h.

By comparing the results given in Fig. 10c with those given for the globally-adaptive mesh in Fig. 7b we observe that the desired tolerance (for the recovered derivative in the subdomain) can be achieved by using a global/local adaptive mesh which has a *fourth* of the degrees of freedom of a globally-adaptive mesh which achieves the same accuracy in the subdomain (although the global energy-norm of the error for the global/local adaptive mesh is large). In Fig. 11a (resp. Fig. 11b) we show the regions in ω_1^h, where the pointwise effectivity-index κ is between 0.8 and 1.2 for the globally-adaptive mesh (resp. global/local adaptive mesh with respect to ω_1^h) shown in Fig. 6d (resp. Fig. 10). We observe that for both grids the effectivity-index is in the range [0.8, 1.2] in large portions of ω_1^h. In the case of the global/local adaptive grid we have $0.8 \le \kappa \le 1.2$ almost over the entire subdomain.

In order to demonstrate the sensitivity of the recovered gradient to the pollution-error we give, in Figs. 12a and 12b, the regions of relative-error in the recovered derivative for the pollution-adaptive meshes with respect to ω_1^h which achieve $\dfrac{\mathcal{M}_{\omega_1^h}}{\mathcal{E}_{\omega_1^h}} = 44.60\%$ and 11.77% respectively. By comparing Fig. 10c, Fig. 12a and

Fig. 12b we observe that when the pollution error in ω_1^h is controlled to a smaller tolerance (relative to the local-error in ω_1^h) there is a substantial gain in the 5%-relative-error regions for the recovered gradient.

In order to achieve the goal $\dfrac{\mathcal{E}_{\omega_1^h}}{\|\nabla u_h\|} \leq 5\%$ we employed an initial grid with mesh-size $h = \dfrac{1}{16}$ in ω_1^h. In Figs. 13a and 13b we show the meshes (from the sequence of pollution-adaptive meshes with respect to ω_1^h, where $h = \dfrac{1}{16}$) for which $\dfrac{\mathcal{M}_{\omega_1^h}}{\mathcal{E}_{\omega_1^h}} = 7.76\%$ and $\dfrac{\mathcal{M}_{\omega_1^h}}{\mathcal{E}_{\omega_1^h}} = 4.47\%$, respectively. In Figs. 14a, 14b we show regions of relative-error in the recovered gradient π_h for the mesh of Fig. 13a, 13b, respectively. As observed earlier, when the pollution error is controlled to a smaller tolerance, there is a significant gain in the 2%-relative-error regions for the recovered-gradient.

Finally, we show that in general we cannot predict a-priori how to refine the mesh in order to control the pollution-error in a given subdomain. We considered the mesh-patch ω_2^h, meshed with uniform-grid with $h = \dfrac{1}{8}$, and constructed the sequence of pollution-adaptive grids with respect to ω_2^h. In Figs. 15a and 15b we give the meshes from this sequence which give $\dfrac{\mathcal{M}_{\omega_2^h}}{\mathcal{E}_{\omega_2^h}} = 5.79\%$ and $\dfrac{\mathcal{M}_{\omega_2^h}}{\mathcal{E}_{\omega_2^h}} = 1.73\%$, respectively. We note that these meshes are refined several times near the corner at C which is far from the subdomain ω_2^h while only a few refinements are employed near the corner at F (which is much closer to the subdomain than C). In Figs. 16a and 16b we give the regions of the relative-error in the recovered gradient in ω_2^h for the meshes shown in Figs. 15a and 15b, respectively. By comparing Fig. 16a and Fig. 9 we note that there is a significant gain in the 4%-relative-error regions when a global/local adaptive mesh is employed instead of a globally-adaptive mesh. Note that the global/local adaptive meshes are much more graded near the singular-points than the globally-adaptive meshes shown in Figs. 6a-6g.

In summary, we observe the following:

1. By controlling the pollution-error to a sufficiently low tolerance in a subdomain of interest we can obtain full gain in the local accuracy of the recovered gradient in that subdomain.

2. When one is interested in obtaining high-accuracy only in a small subdomain, global/local adaptive meshes with respect to the region of interest are, in general, much more economical than globally-adaptive meshes.

3. In general, *we cannot say a-priori* how to refine the mesh in order to control the pollution-error in a region of interest.

19

5 Conclusions

We studied the effect of the pollution-error on the pointwise quality of the recovered derivatives in the interior of the mesh. We observed the following:

1. When quasi-uniform meshes, or meshes which are locally refined only in the subdomain, are employed it may not be possible to achieve better accuracy (than the finite element solution) by using a local recovery in a subdomain of interest.

2. When a globally-adaptive mesh is employed, the local quality of the recovery can be ensured only for a sufficiently low tolerance for the global energy-norm. Such meshes may be very expensive when one is interested to achieve good accuracy only in a local region.

3. By employing global/local adaptive meshes we can control the pollution-error (to within any prescribed tolerance) in any patch of elements of interest and we can obtain higher-order accuracy (relative to the finite element solution) by employing a local recovery.

4. For the boundary-value problems which occur in practical computations (which include many corner points) desired local accuracies can be achieved with much fewer degrees of freedom by employing global/local-adaptive meshes instead of globally-adaptive meshes.

6 Acknowledgments

References

1. I. Babuška, T. Strouboulis, A. Mathur and C.S. Upadhyay, 'Pollution error in the h-version of the finite element method and the local quality of a-posteriori error estimators', *Technical Note BN-1163*, Institute for Physical Science and Technology, University of Maryland, College Park, February 1994 (to appear in Finite Elements in Analysis and Design, 1995).

2. I. Babuška, T. Strouboulis, C.S. Upadhyay and S.K. Gangaraj, 'A-posteriori estimation and adaptive control of the pollution-error in the h-version of the finite element method', Technical Note BN-1175, Institute for Physical Science and Technology, University of Maryland, College Park, August 1994 (to appear in the Int. J. Numer. Methods Engrg., 1995).

3. O.C. Zienkiewicz and J.Z. Zhu, 'The superconvergent patch recovery and a posteriori error estimates. Part 1: The recovery technique', *Internat. j. numer. methods engrg.* 33 (1992) 1331-1364.

4. O.C. Zienkiewicz and J.Z. Zhu, 'The superconvergent patch recovery and a posteriori error estimates. Part 2: Error estimates and adaptivity', *Internat. j. numer. methods engrg.* 33 (1992) 1365-1382.

5. I. Babuška, T. Strouboulis, S.K. Gangaraj and C.S. Upadhyay, 'Validation of recipes for the recovery of stresses and derivatives by a computer-based approach', *Math. Comput. Modelling* 20 (1994) 45-89.

6. L.B. Wahlbin, 'Local behavior in finite element methods', in: P.G. Ciarlet and J.L. Lions, eds., Handbook of Numerical Analysis, Vol. II (North-Holland, Amsterdam, 1991) 357-522.

7. I. Babuška, T. Strouboulis, C.S. Upadhyay and S.K. Gangaraj, 'A model study of element residual estimators for linear elliptic problems: The quality of the estimators in the interior of meshes of triangles and quadrilaterals', *Technical Note BN-1171*, Institute for Physical Science and Technology, University of Maryland, College Park, May 1994.

8. P. Ladeveze and D. Leguillon, 'Error estimate procedure in the finite element method and applications', *SIAM J. Numer. Anal.* 20 (1983) 485-509.

9. M. Ainsworth and J.T. Oden, 'A unified approach to a-posteriori error estimation using element residual methods', *Numer. Math.* 65 (1993) 23-50.

10. I. Babuška and W.C. Rheinboldt, 'Reliable error estimation and mesh adaptation for the finite element method', in: J.T. Oden, ed., Computational Methods in Nonlinear Mechanics (North-Holland, Amsterdam, 1980) 67-108.

11. O.C. Zienkiewicz, J.Z. Zhu and N.G. Gong, 'Effective and practical *h-p*-version adaptive analysis procedures for the finite element method', *Internat. J. Numer. methods engrg.* 28 (1989) 879-891.

12. J. Hugger, 'Recovery and few parameter representation of the optimal density function for near optimal finite element meshes', *Comput. Methods Appl. Mech. Engrg.* 109 (1993) 41-71.

13. J. Fish and S. Markolefas, 'Adaptive global-local refinement strategy based on the interior error estimates of the *h*-method', *Internat. J. numer. methods engrg.* 37 (1994) 827-838.

14. J.B. Ransom and N.F. Knight Jr., 'Global/Local analysis for composite panels', *Computers & Structures* 37 (1990) 375-395.

15. M.A. Aminpour, S.L. McCleary, J.B. Ransom and J.M. Housner, 'A global/local analysis for treating details structural design, in Adaptive, Multilevel and Hierarchical Computational Strategies', A.K. Noor, ed. *AMD-Vol. 157*, pp. 119-137, American Society of Mechanical Engineers, New York, 1992.

16. M.A. Aminpour, J.B. Ransom and S.L. McCleary, 'Coupled analysis of independently modeled finite element subdomains', in the *Proceedings of the 33rd AIAA Structures, Structural Dynamics and Materials Conference, Part 1, Structures I*, pp. 109-120, American Institute of Astronautics and Aeronautics, 1992.

17. I. Babuška, R.B. Kellog and J. Pitkäranta, Direct and inverse error estimates for finite elements with mesh refinements, *Numer. Math.* 33 (1979) 447-471.

List of Figures

(a) The regions of 0.5%, 1%, 2% (dark gray, gray, light gray) for ρ_h, the relative-error in the gradient of the finite element solution;

(b) The regions of 0.5%, 1%, 2% (dark gray, gray, light gray) for π_h, the relative-error in the recovered gradient.

Note that *there is a significant gain in the 2%-regions when the recovered gradient is employed instead of the gradient of the finite-element solution.*

Fig. 9. The regions of 1%, 2%, 4% (dark gray, gray, light gray) for the relative-error in the recovered gradient in the subdomain ω_2^h for the globally-adaptive mesh shown in Fig. 6d.

Fig. 10. The mesh and the corresponding regions of relative-error obtained using the global/local adaptive algorithm:

(a) The mesh of biquadratic elements which achieves $\dfrac{\mathcal{E}_{\omega_1^h}}{\|\nabla u_h\|_{\omega_1^h}} = 9.18\%$ and

$\dfrac{\mathcal{M}_{\omega_1^h}}{\mathcal{E}_{\omega_1^h}} = 19.13\%$. The subdomain ω_1^h is shown shaded gray.

(b) The regions of 2.5%, 5%, 10% (dark gray, gray, light gray) for the relative-error in the gradient of the finite element solution ρ_h.

(c) The regions of 2.5%, 5%, 10% (dark gray, gray, light gray) for the relative-error in the recovered gradient π_h.

Note that *the 10%-regions for π_h are significantly larger than those given in Fig. 7b for the global-adaptive mesh.* Note also that *the mesh around the corner-point at F is left completely unrefined.*

Fig. 11. The pointwise effectivity index for the recovered gradient, $\kappa(x)$. The regions where $0.8 \leq \kappa(x) \leq 1.2$ are shown shaded gray for:

(a) The subdomain ω_1^h given in Fig. 6d for the globally adaptive mesh;

(b) The subdomain ω_1^h given in Fig. 10a for the global/local adaptive mesh with respect to ω_1^h.

Note that *in the case of the global/local adaptive mesh, we have $0.8 \leq \kappa \leq 1.2$ almost over the entire subdomain.*

Fig. 12. The regions of 2.5%, 5%, 10% (dark gray, gray, light gray) for the relative-error in the recovered gradient π_h in ω_1^h for global/local adaptive meshes with respect to ω_1^h for which the following tolerances were achieved:

(a) $\dfrac{\mathcal{E}_{\omega_1^h}}{\|\nabla u_h\|_{\omega_1^h}} = 7.87\%$ and $\dfrac{\mathcal{M}_{\omega_1^h}}{\mathcal{E}_{\omega_1^h}} = 44.60\%$;

(b) $\dfrac{\mathcal{E}_{\omega_1^h}}{\|\nabla u_h\|_{\omega_1^h}} = 9.62\%$ and $\dfrac{\mathcal{M}_{\omega_1^h}}{\mathcal{E}_{\omega_1^h}} = 11.77\%$.

Note that *when the pollution-error in ω_1^h was controlled to a smaller tolerance, there is significant gain in the 5%-relative-error regions.*

Fig. 13. Global/local adaptive meshes of biquadratic elements with respect to ω_1^h achieving the following tolerances:

(a) $\dfrac{\mathcal{E}_{\omega_1^h}}{\|\nabla u_h\|_{\omega_1^h}} = 2.62\%$ and $\dfrac{\mathcal{M}_{\omega_1^h}}{\mathcal{E}_{\omega_1^h}} = 7.76\%$;

(b) $\dfrac{\mathcal{E}_{\omega_1^h}}{\|\nabla u_h\|_{\omega_1^h}} = 4.13\%$ and $\dfrac{\mathcal{M}_{\omega_1^h}}{\mathcal{E}_{\omega_1^h}} = 4.47\%$.

Note that *the mesh near the corner-point F is also refined several times (compared to the mesh shown in Fig. 10a where the mesh near F is left unrefined)*.

Fig. 14. The regions of 0.5%, 1%, 2% (dark gray, gray and light gray) for the relative-error in the recovered gradient π_h in ω_1^h. The regions are given for the global-local adaptive meshes shown in: (a) Fig. 13a; (b) Fig. 13b.

Fig. 15. Global/local adaptive meshes of biquadratic elements with respect to ω_2^h achieving the following tolerances:

(a) $\dfrac{\mathcal{E}_{\omega_2^h}}{\|\nabla u_h\|_{\omega_2^h}} = 3.28\%$ and $\dfrac{\mathcal{M}_{\omega_2^h}}{\mathcal{E}_{\omega_2^h}} = 5.79\%$;

(b) $\dfrac{\mathcal{E}_{\omega_2^h}}{\|\nabla u_h\|_{\omega_2^h}} = 4.00\%$ and $\dfrac{\mathcal{M}_{\omega_2^h}}{\mathcal{E}_{\omega_2^h}} = 1.73\%$.

We note that *the mesh is refined several times near the corner at C (which is far from the subdomain ω_2^h) while only a few refinements are employed near the corner at F (which is much closer to the subdomain than C)*.

Fig. 16. The regions of relative-error in the recovered gradient in ω_2^h for the global/local adaptive meshes with respect to ω_2^h shown in Fig. 15:

(a) The regions for 1%, 2%, 4% (dark gray, gray, light gray) for the mesh shown in Fig. 15a which has pollution-error of 5.79%;

(b) The regions for 0.25%, 0.3%, 1% (dark gray, gray, light gray) for the mesh shown in Fig. 14b which has pollution-error of 1.73%.

Note that *there is a significant gain in the 1%-relative-error regions when the pollution-error is controlled to a smaller tolerance*.
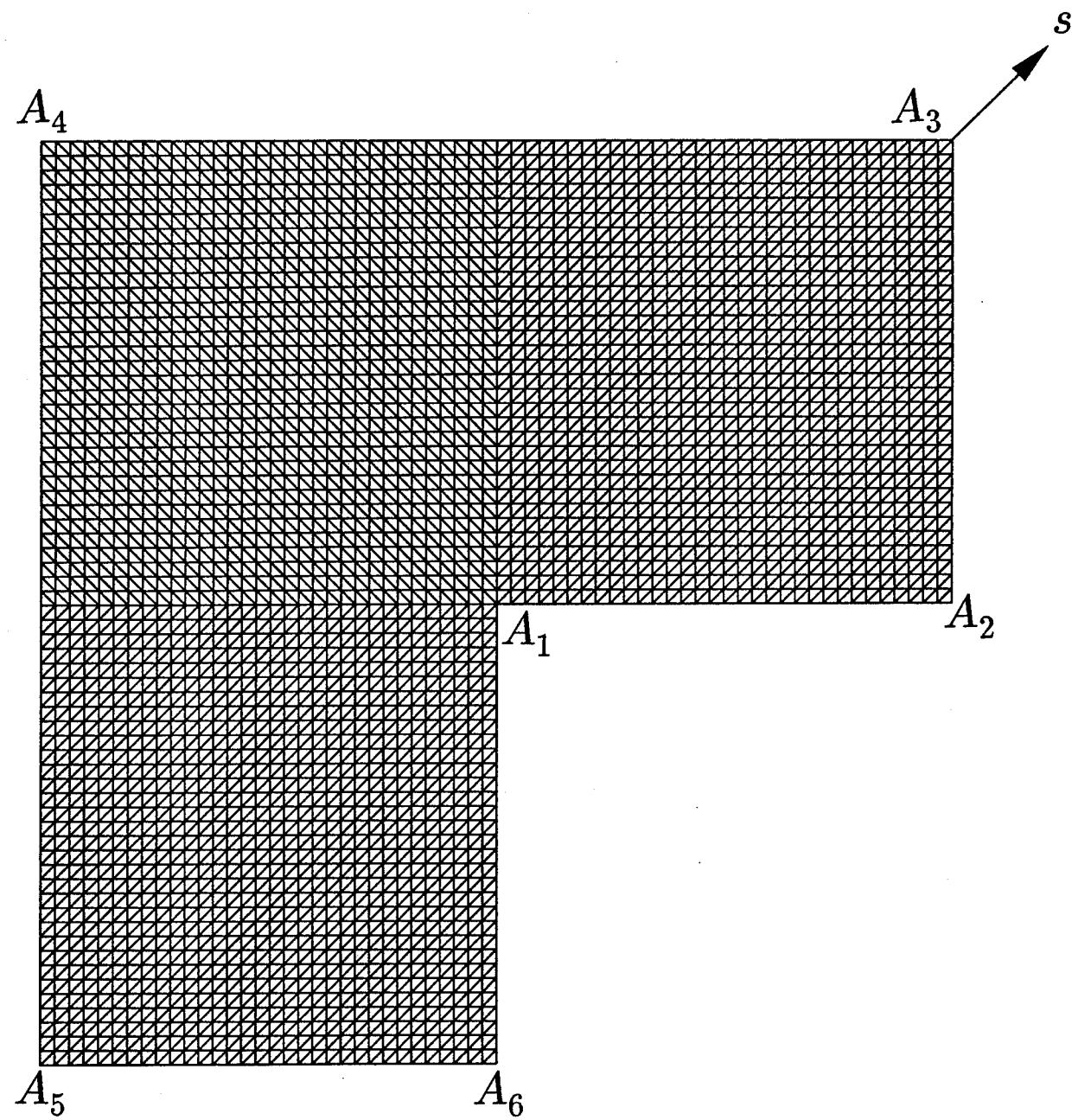
Fig. 1a

Study of the Pollution Error
Singular Solution: $u_{EX}(r,\Theta) = r^{(2/3)} \, Sin(2\Theta/3)$
Quadratic Elements, Uniform Mesh (h = 0.03125)

⊖⊖⊖⊖⊖ Local Error V_1
□□□□□ Pollution Error V_2
△△△△△ Estimated Error using
recovered derivatives

Directional Derivative of the Error

Arc Length Coordinates Along S-Axis

Fig. 1b

τ_{in}

$\mathbf{n}$

τ_{out}

ϵ
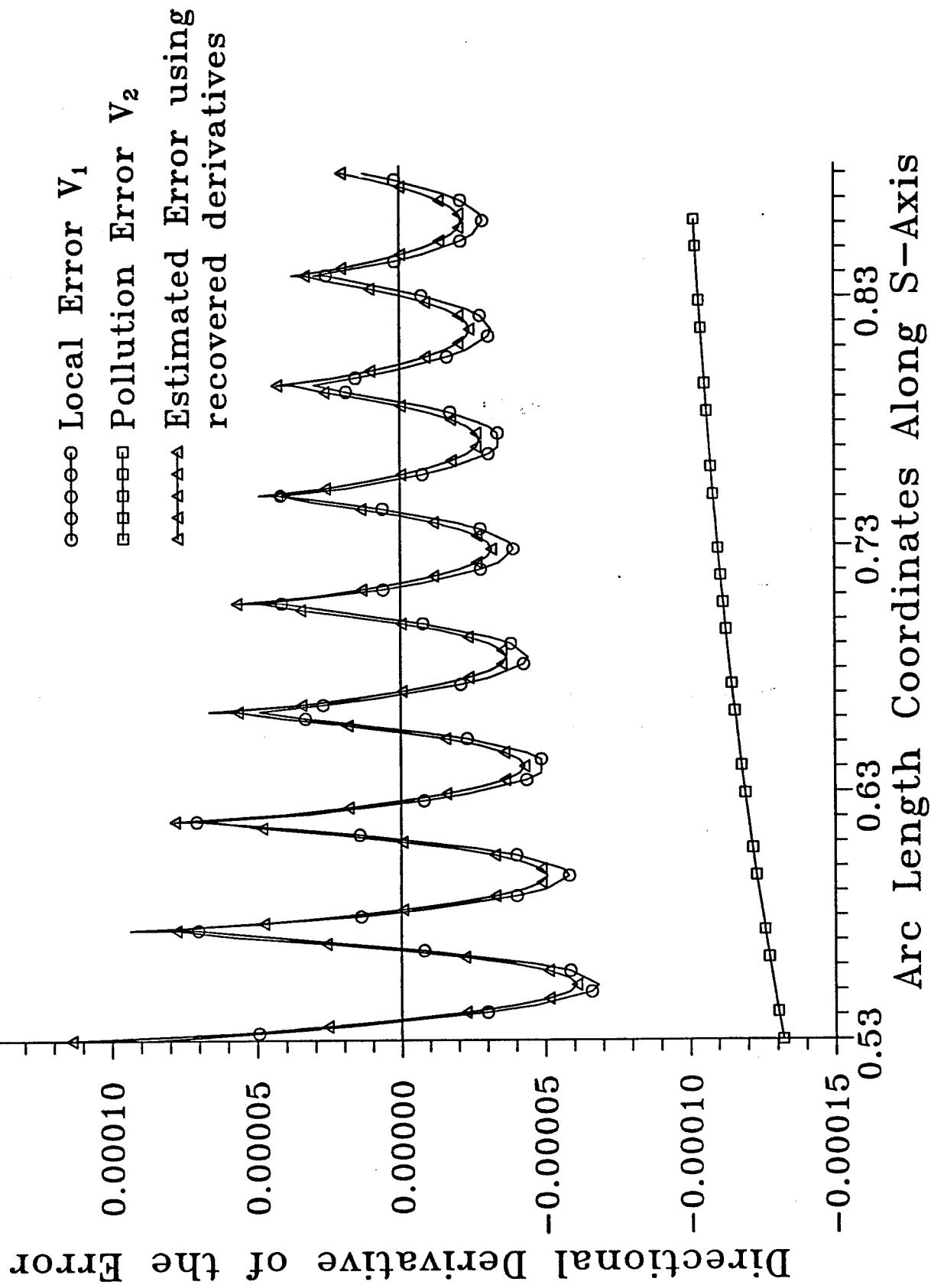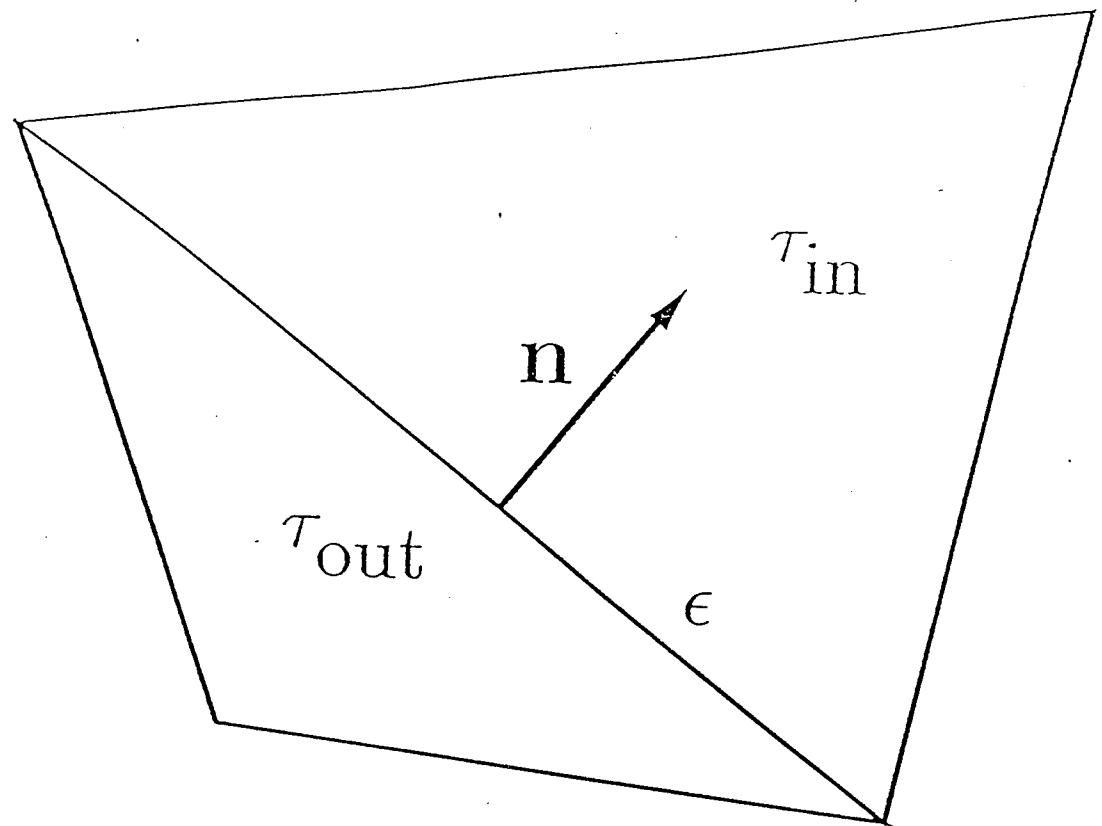
Fig. 2
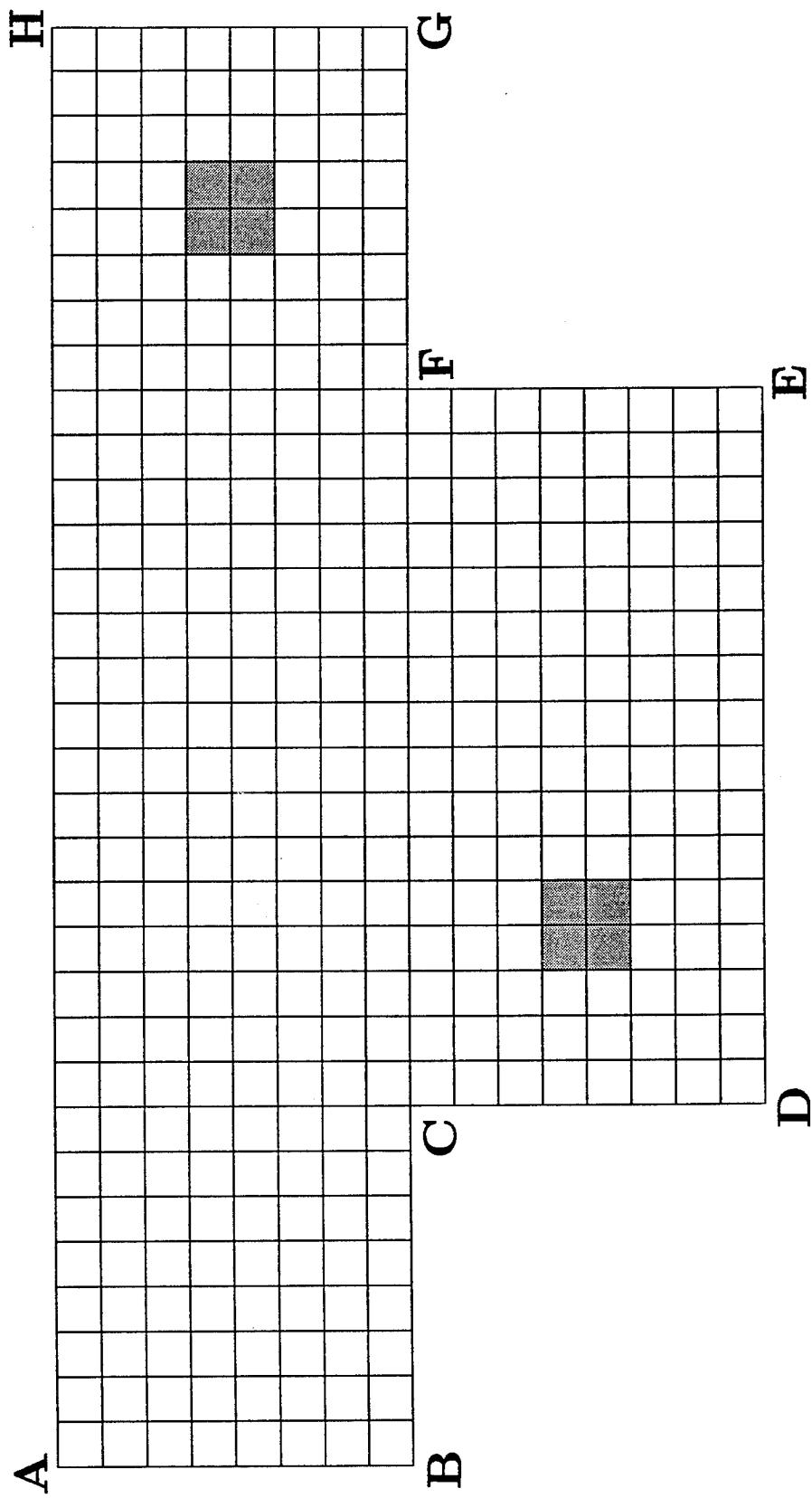
Fig. 3

NDOF = 1633

Fig. 4

NDOF = 4745

Globally Adaptive Meshes
Global/Local Adaptive Meshes

LOG[(Number of degrees of freedom)$^{1/2}$]

LOG(‖e‖)

T_1 T_2 T_3 T_4 T_5 T_6 T_7

2
1
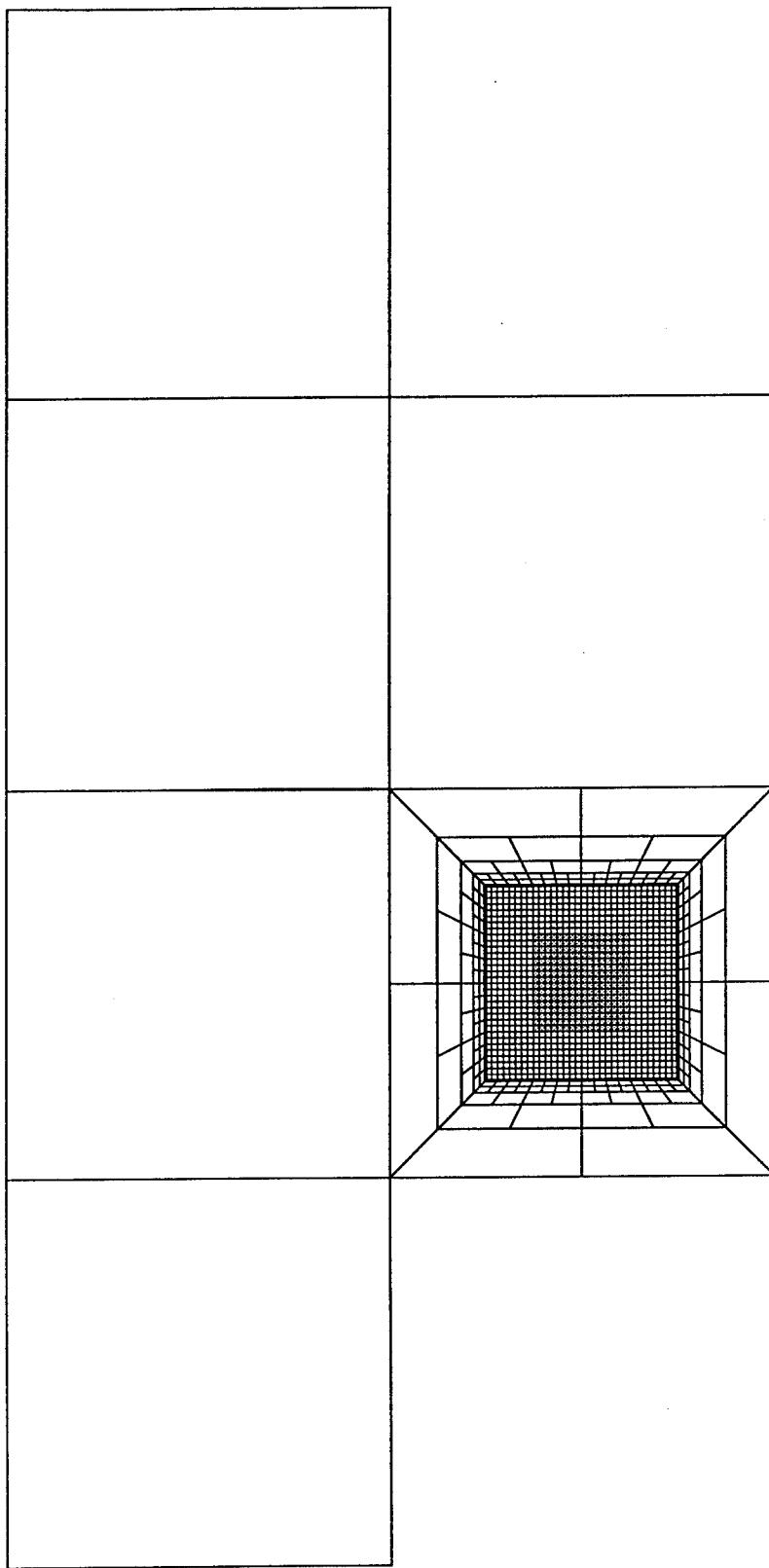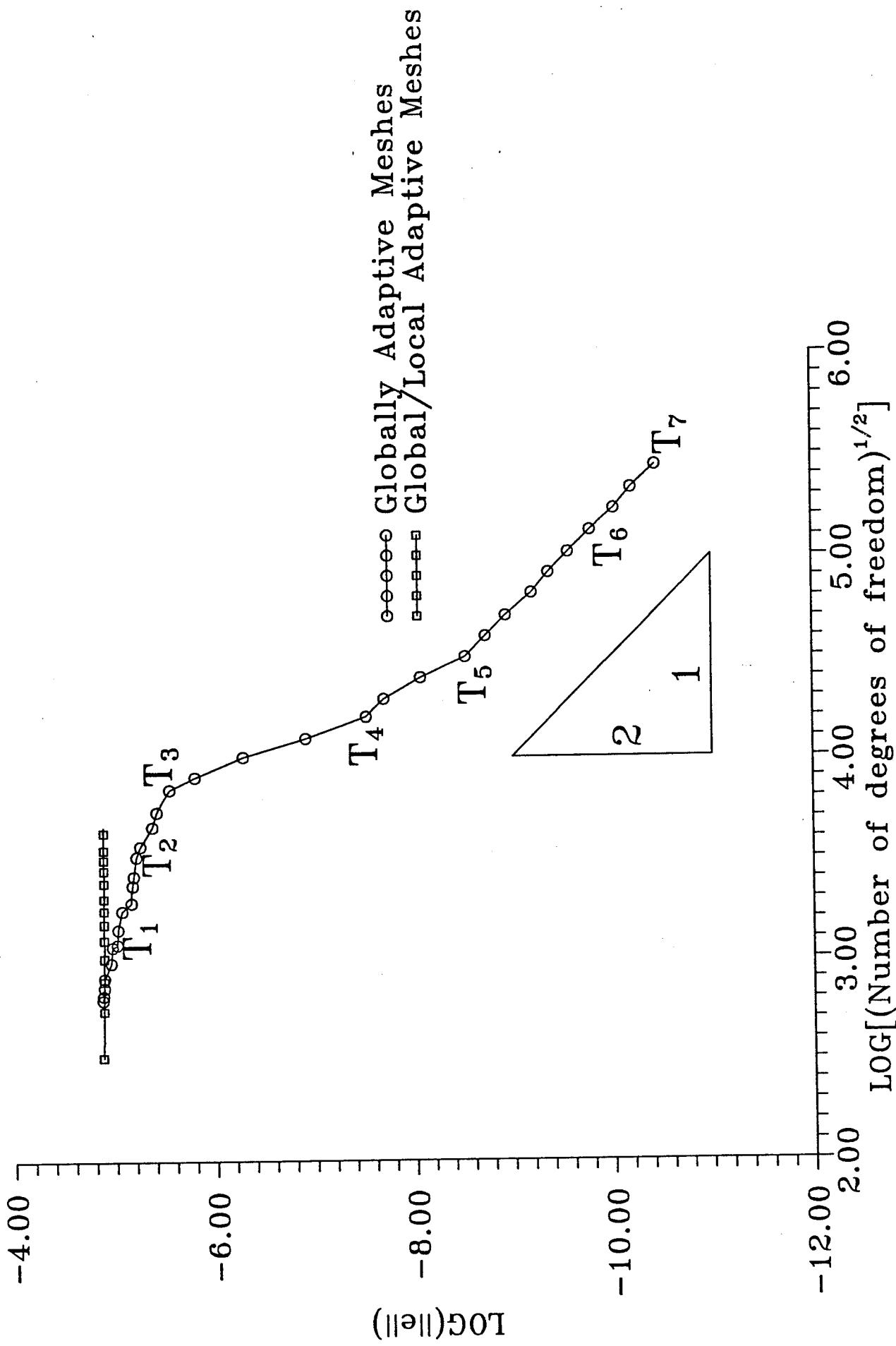
Fig. 5
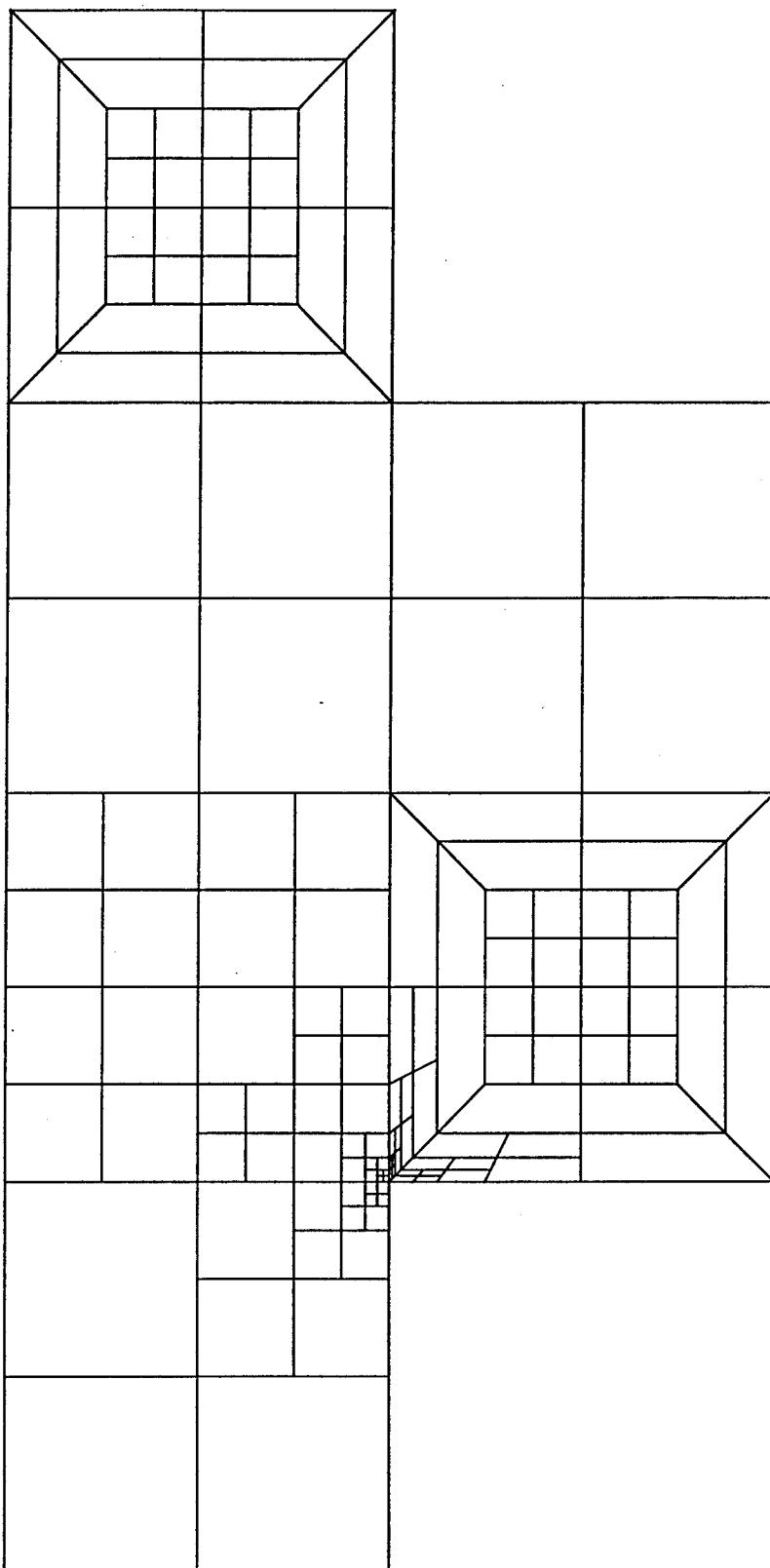
NDOF = 549

Fig. 6a
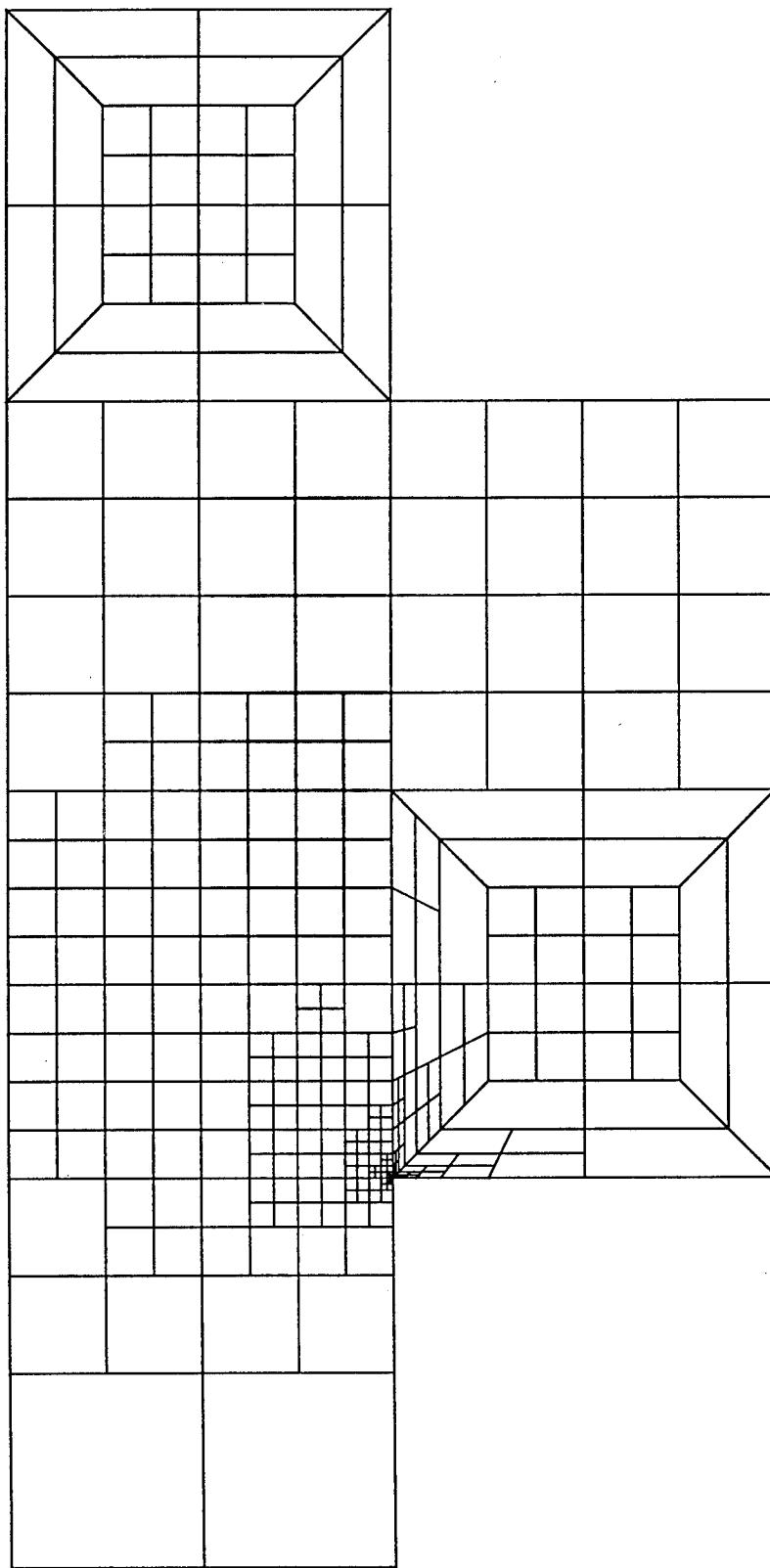
Fig. 6b

NDOF = 1257
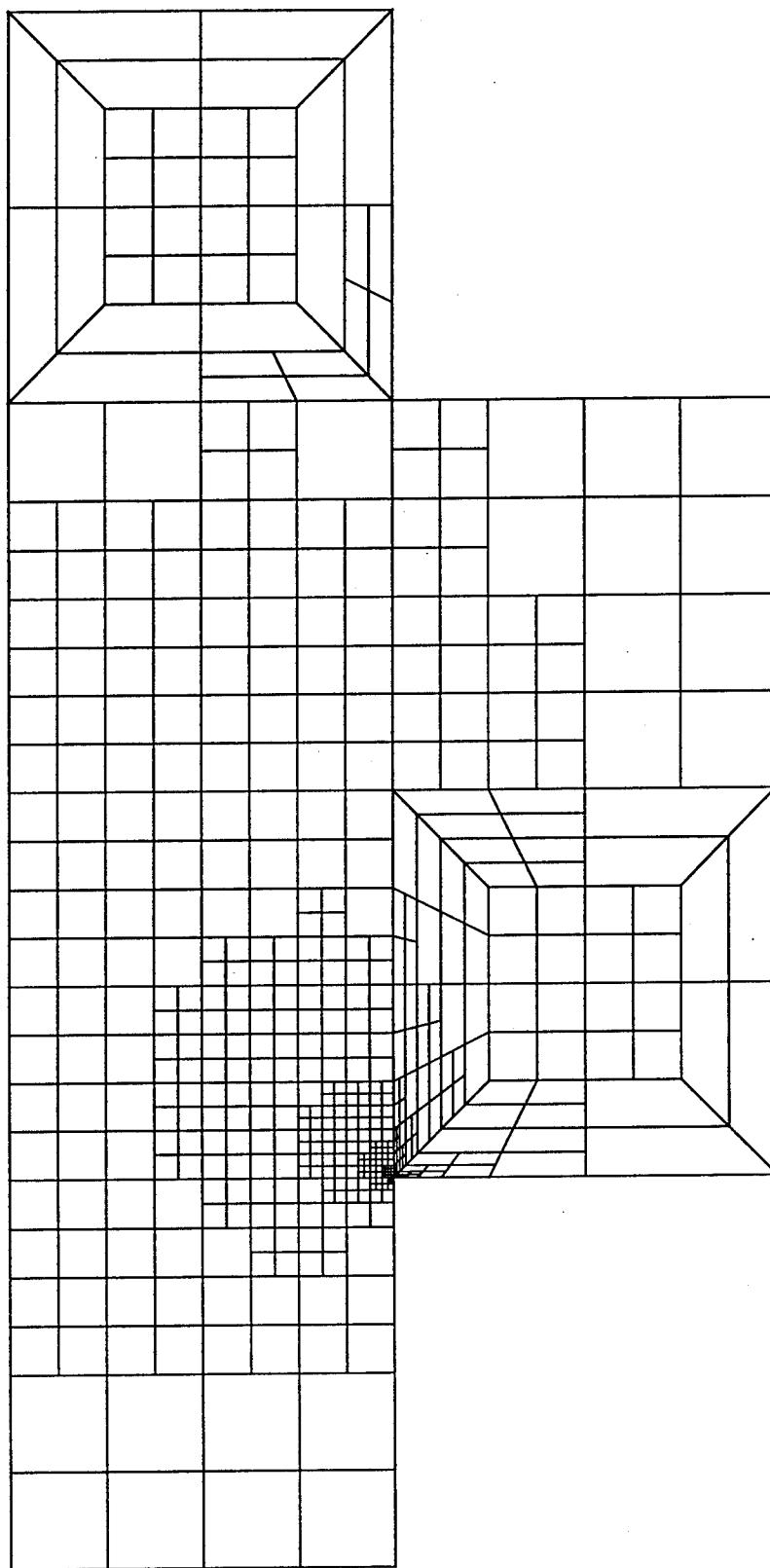
Fig. 6c

NDOF = 2197
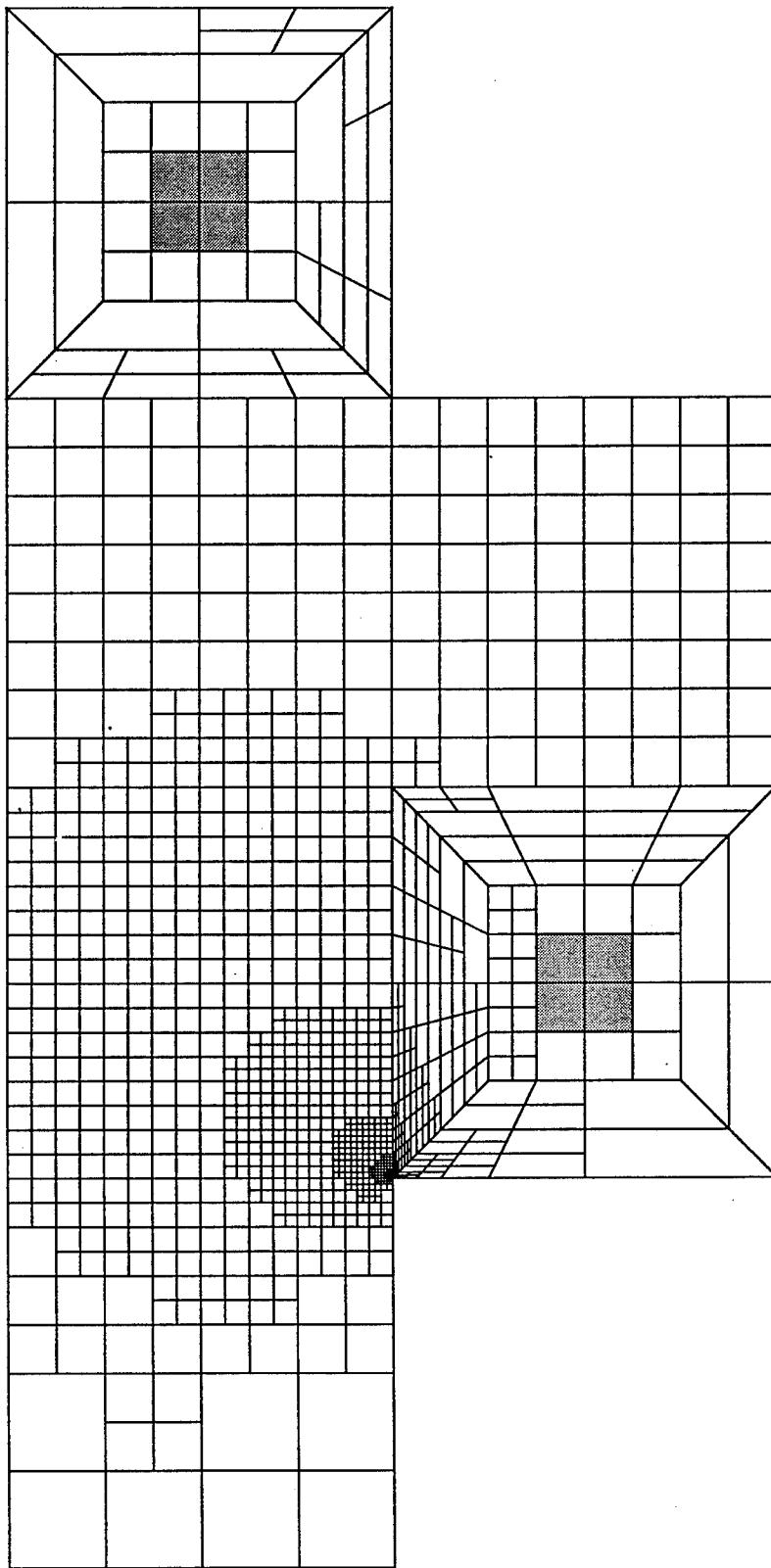
Fig. 6d

NDOF = 4489
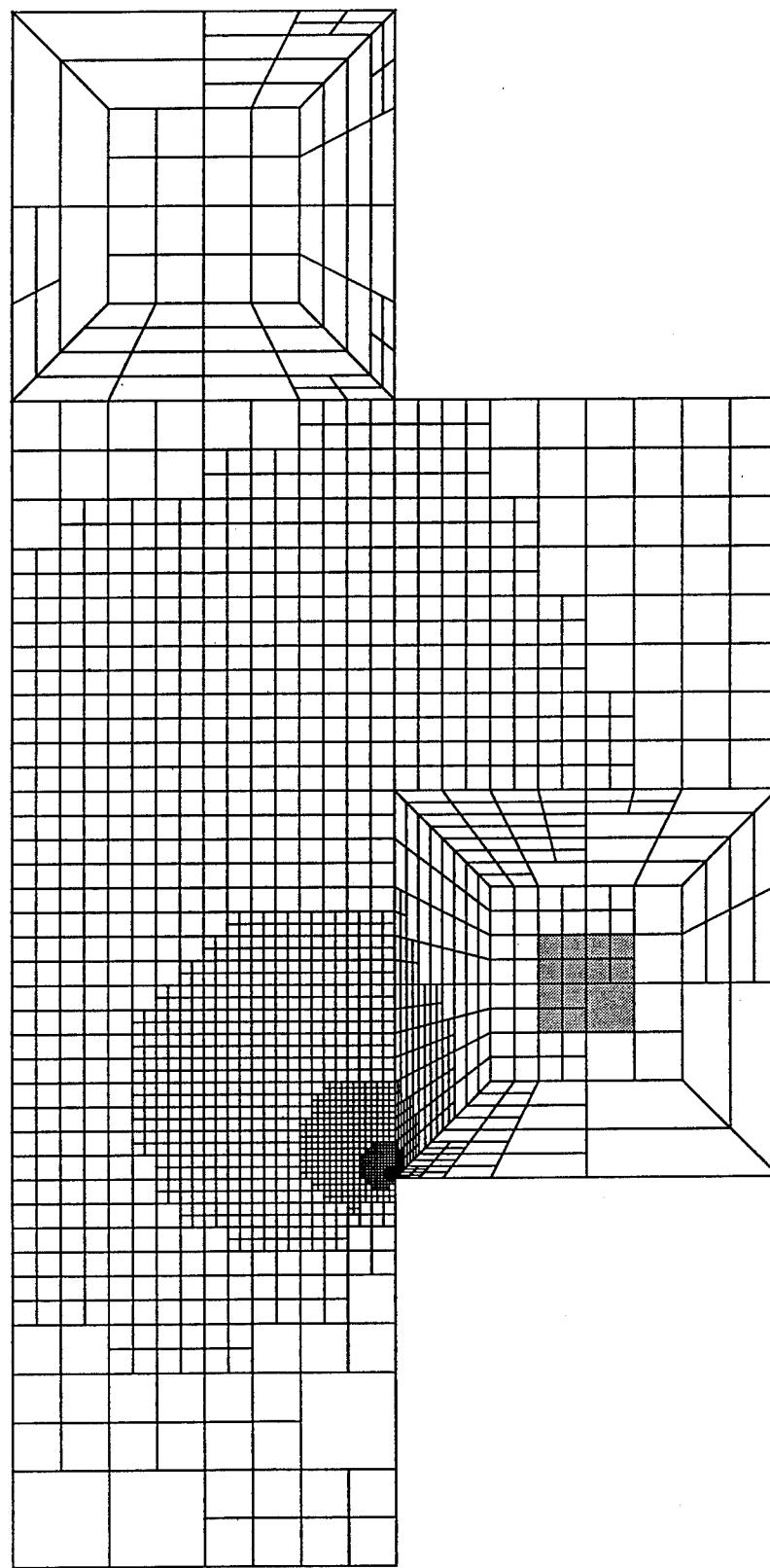
Fig. 6e

NDOF = 8119
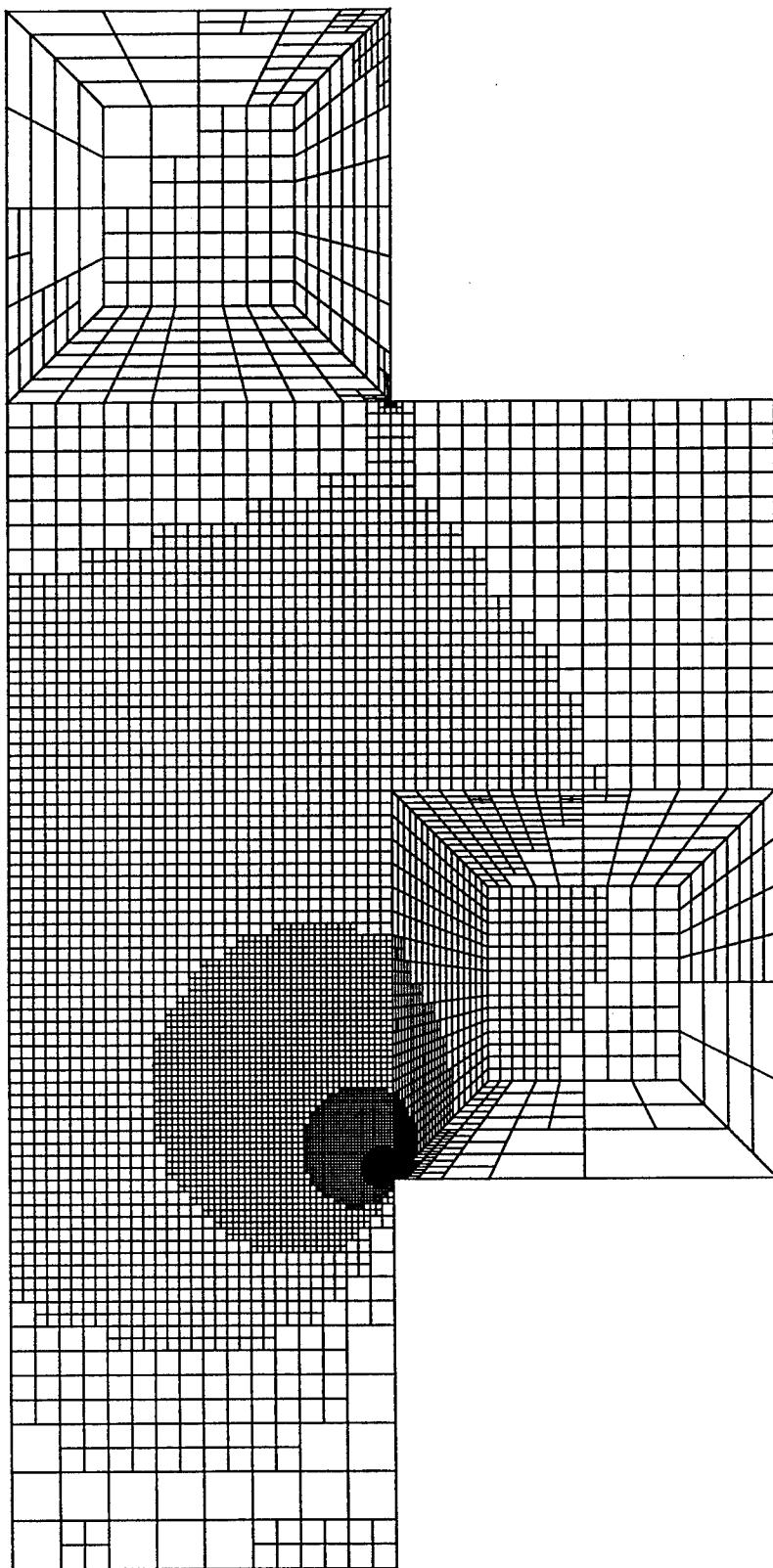
Fig. 6f

NDOF = 28593
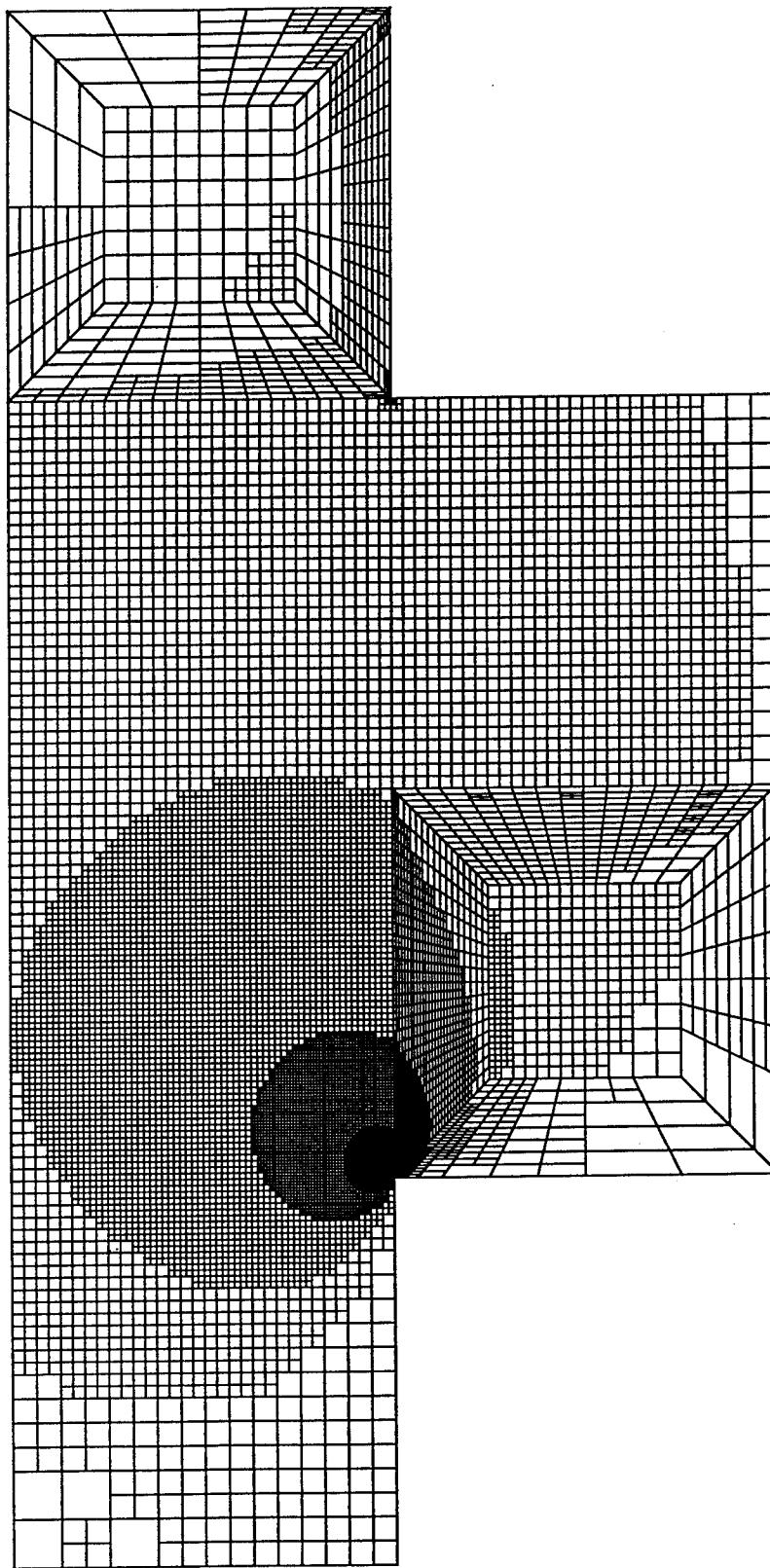
Fig. 6g

NDOF = 54067
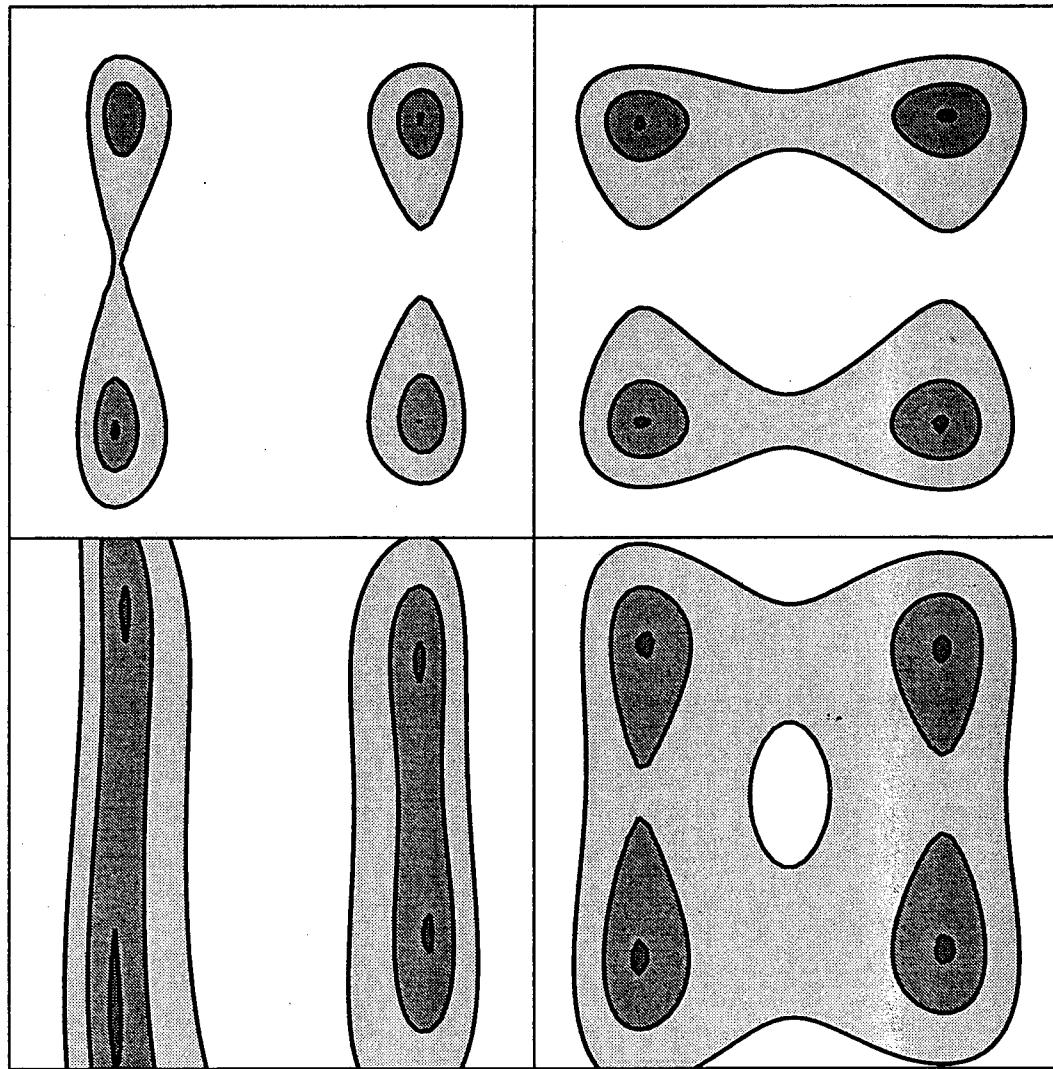
lle_hll/llull = 4.77% , FE-error
Regions of 2.5% , 5% , 10%
MIN = 0.014 , MAX = 0.282

Fig. 7a
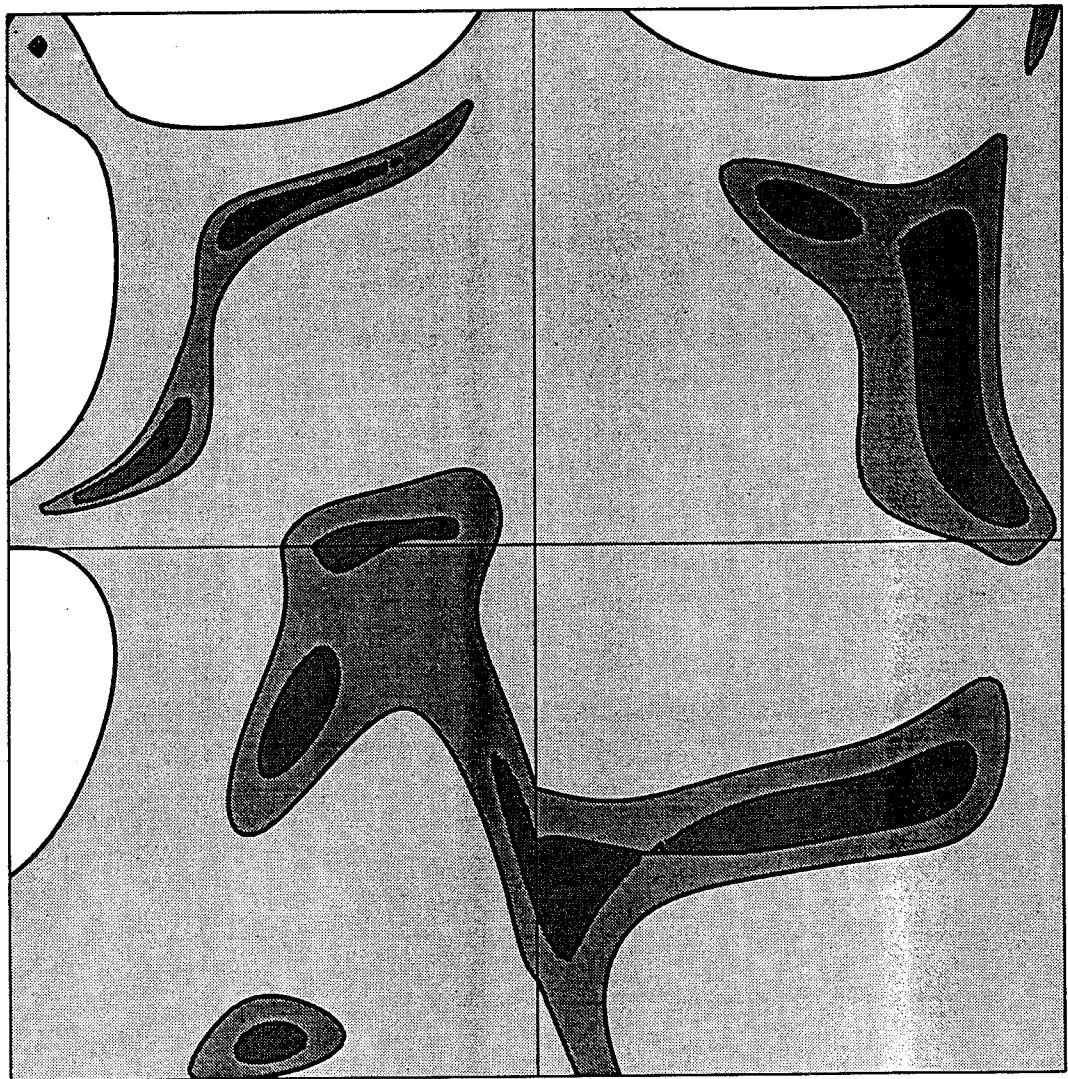
||e_h||/||u|| = 4.77% , ZZ-error
Regions of 2.5% , 5% , 10%
MIN = 0.012 , MAX = 0.224

Fig. 7b
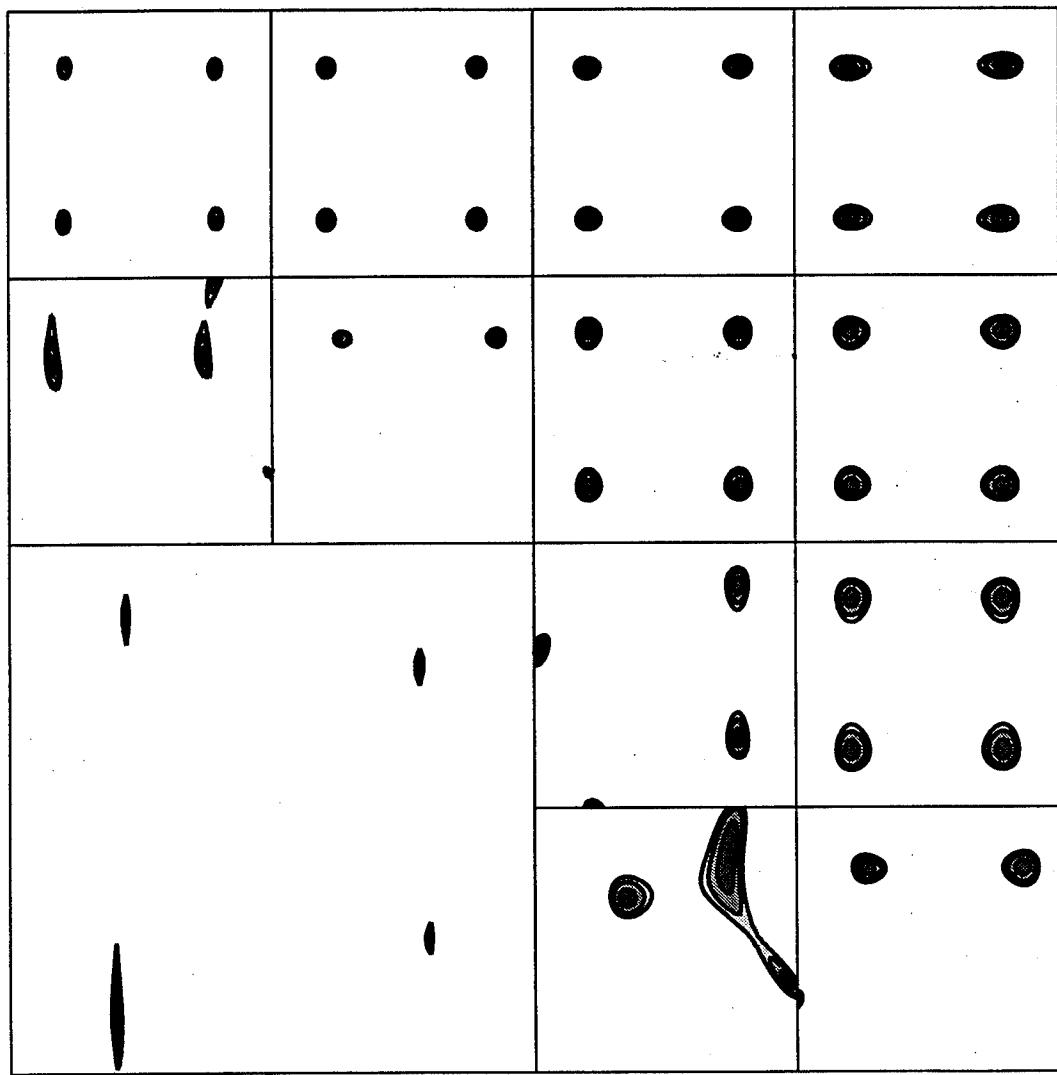
||e_h||/||u|| = 0.93% , FE error
Regions of 0.5% , 1% , 2%

Fig. 8a
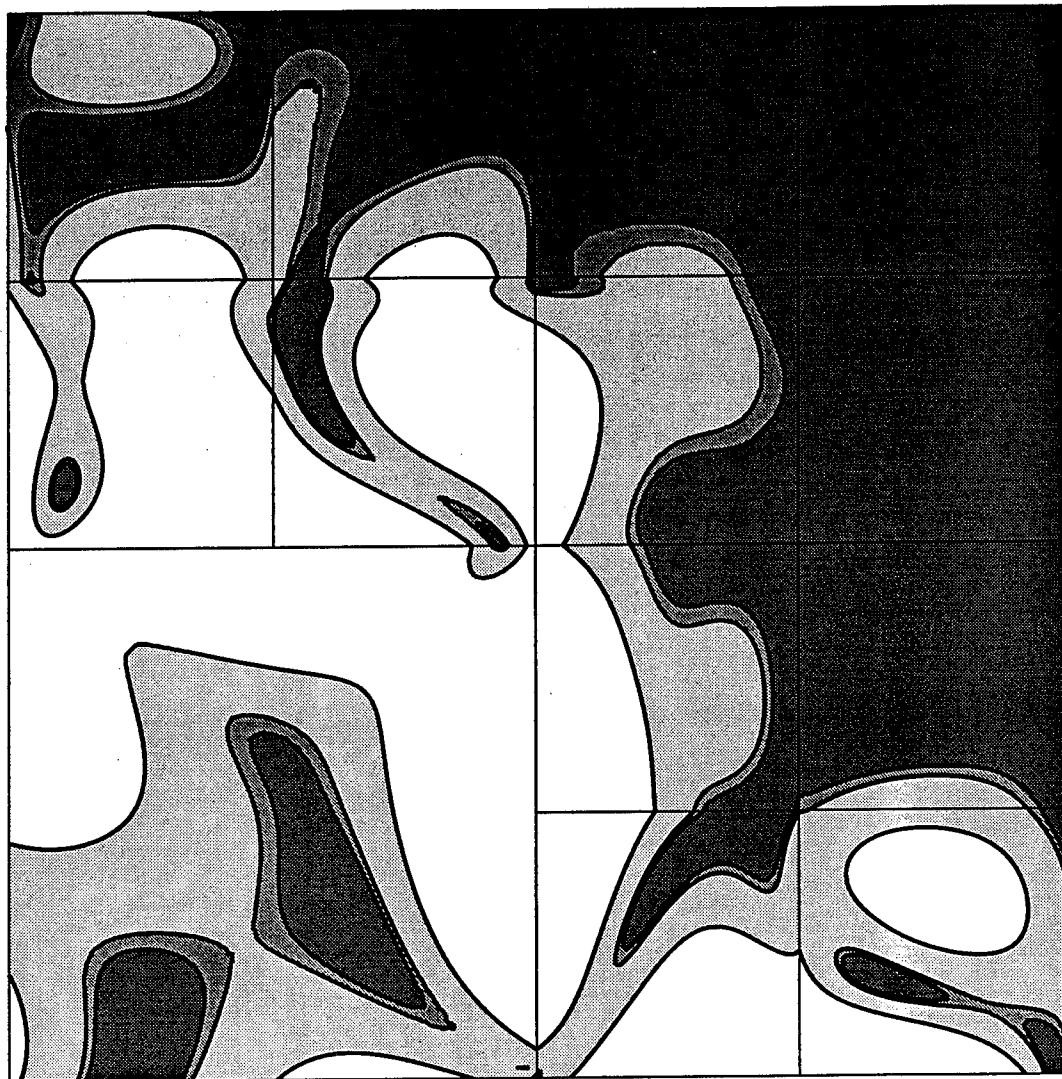
‖e_h‖/‖u‖ = 0.93% , ZZ-error
Regions of 0.5% , 1% , 2%
MIN = 0.00009 , MAX = 0.027

Fig. 8b
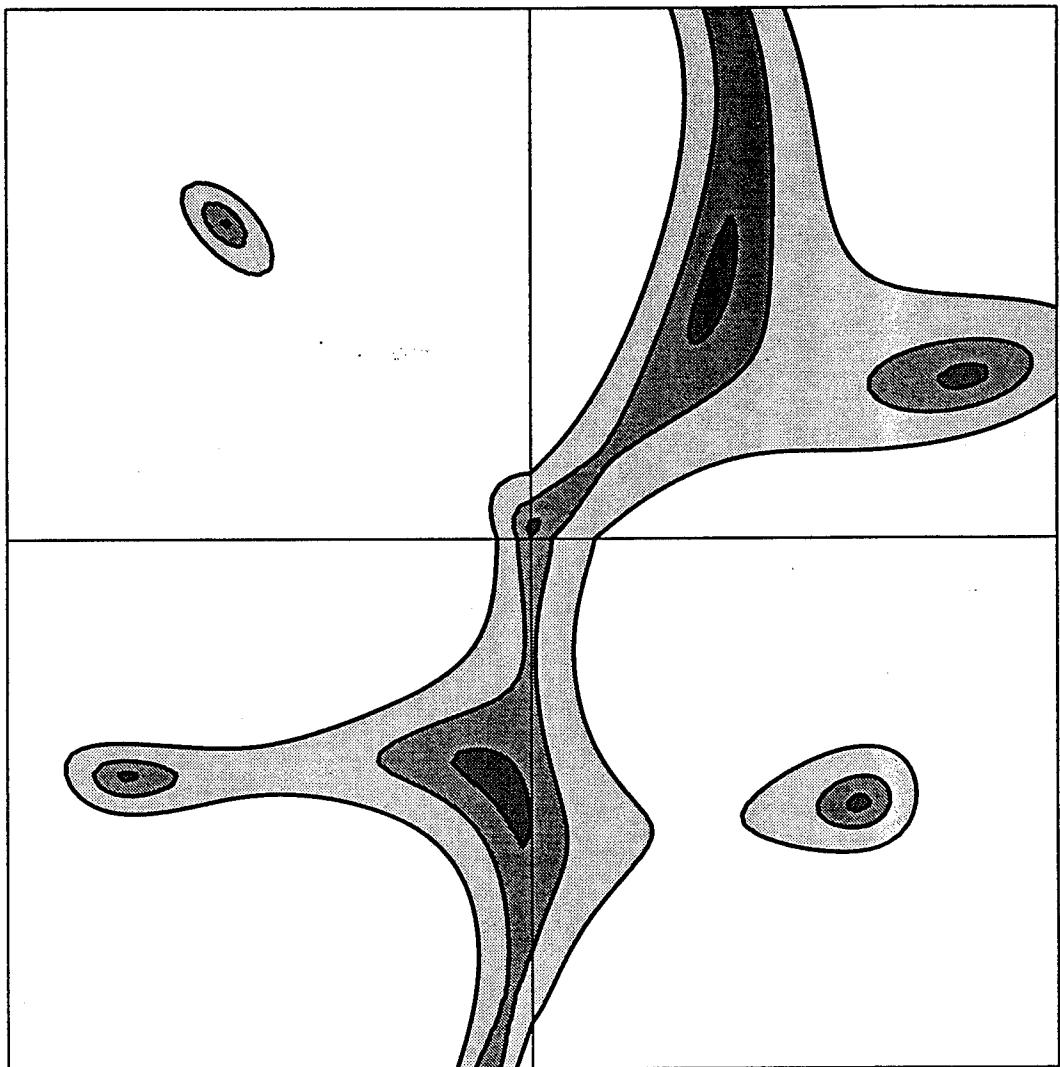
‖e_h‖/‖u‖ = 4.77% , ZZ-error
Regions of 1.0% , 2% , 4%
MIN = 0.006 , MAX = 0.146
Patch 2

Fig. 9
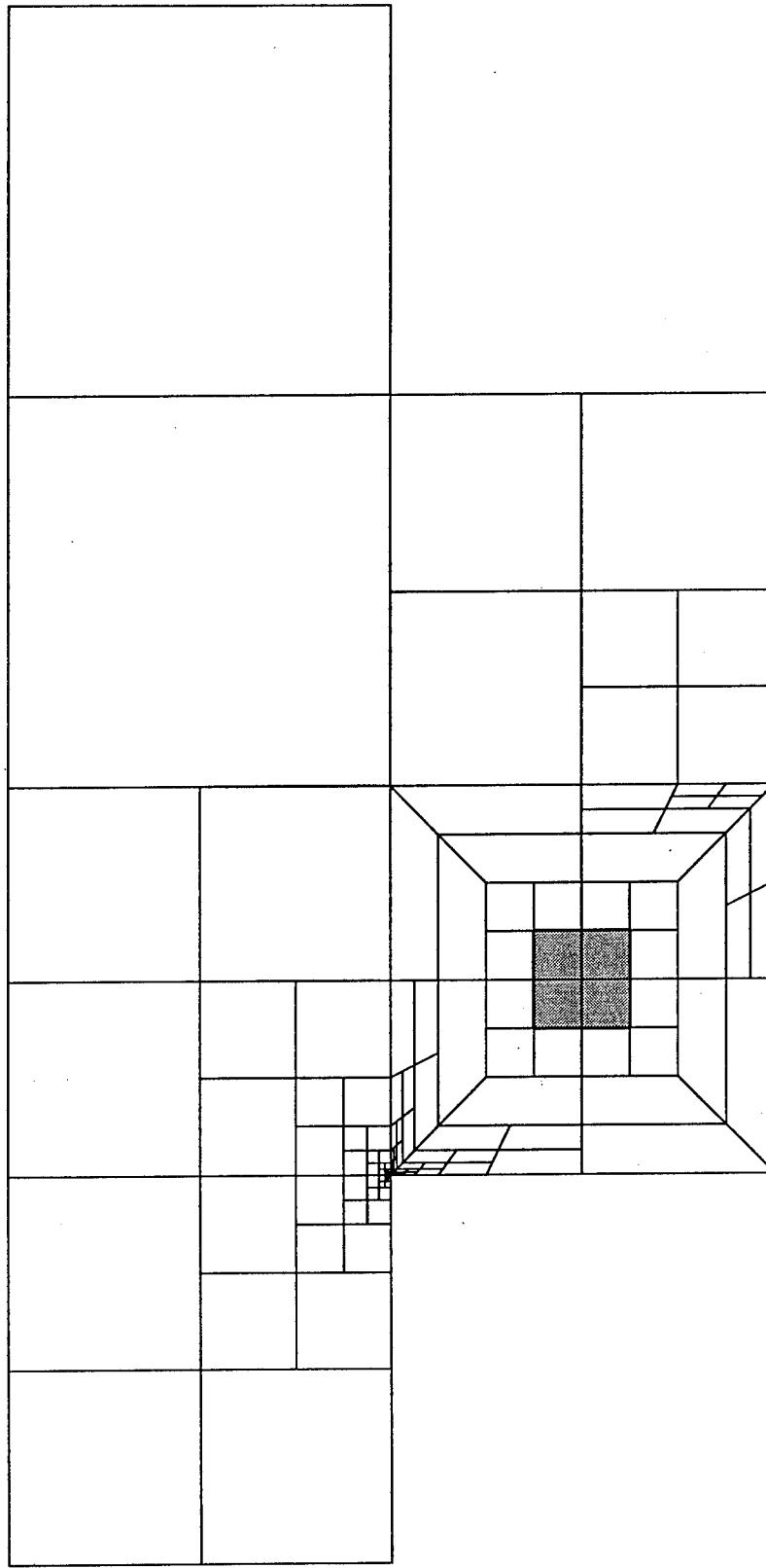
Fig. 10a

NDOF = 1053
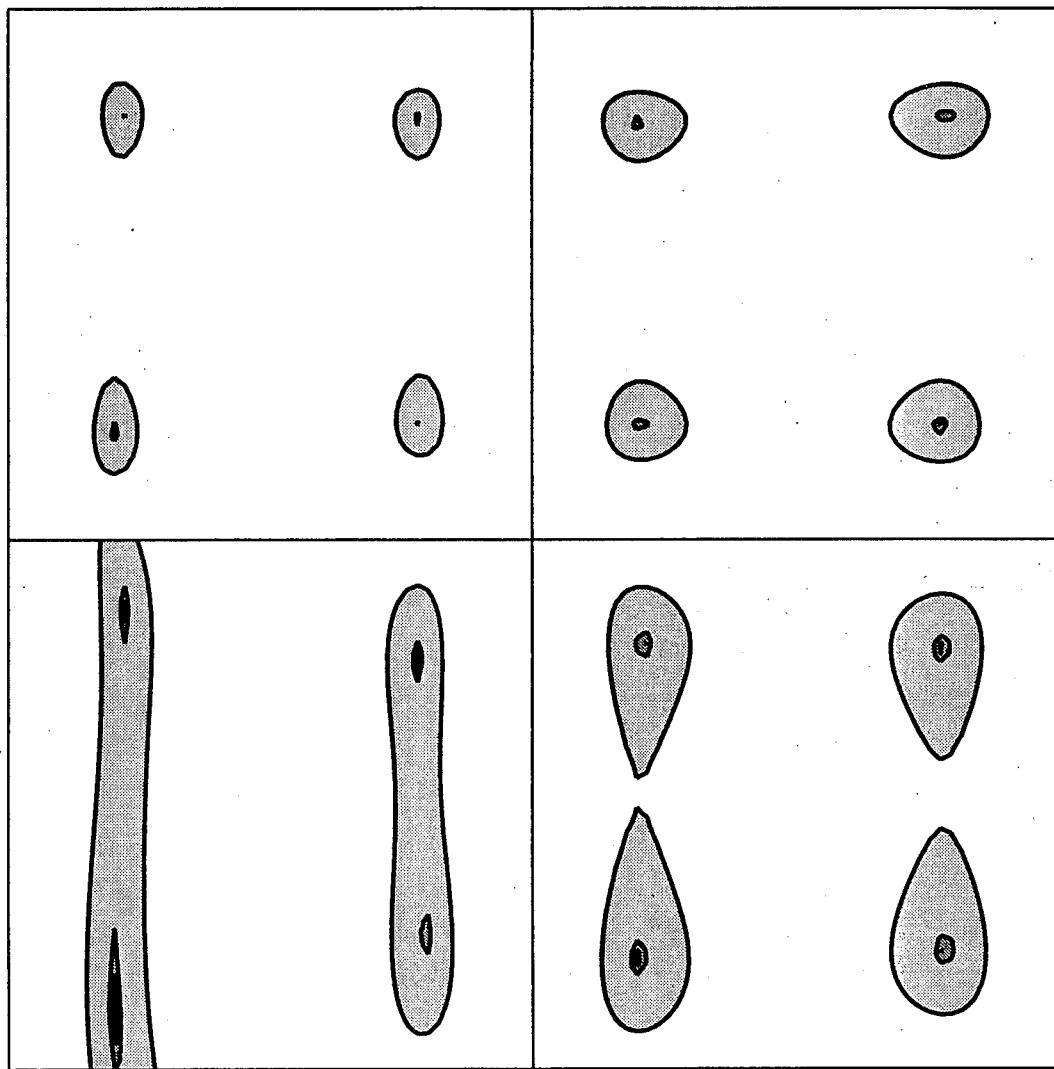
||V2||/eta = 19.13% , FE-error
Regions of 2.5% , 5% , 10%
MIN = 0.009 , MAX = 0.299

Fig. 10b
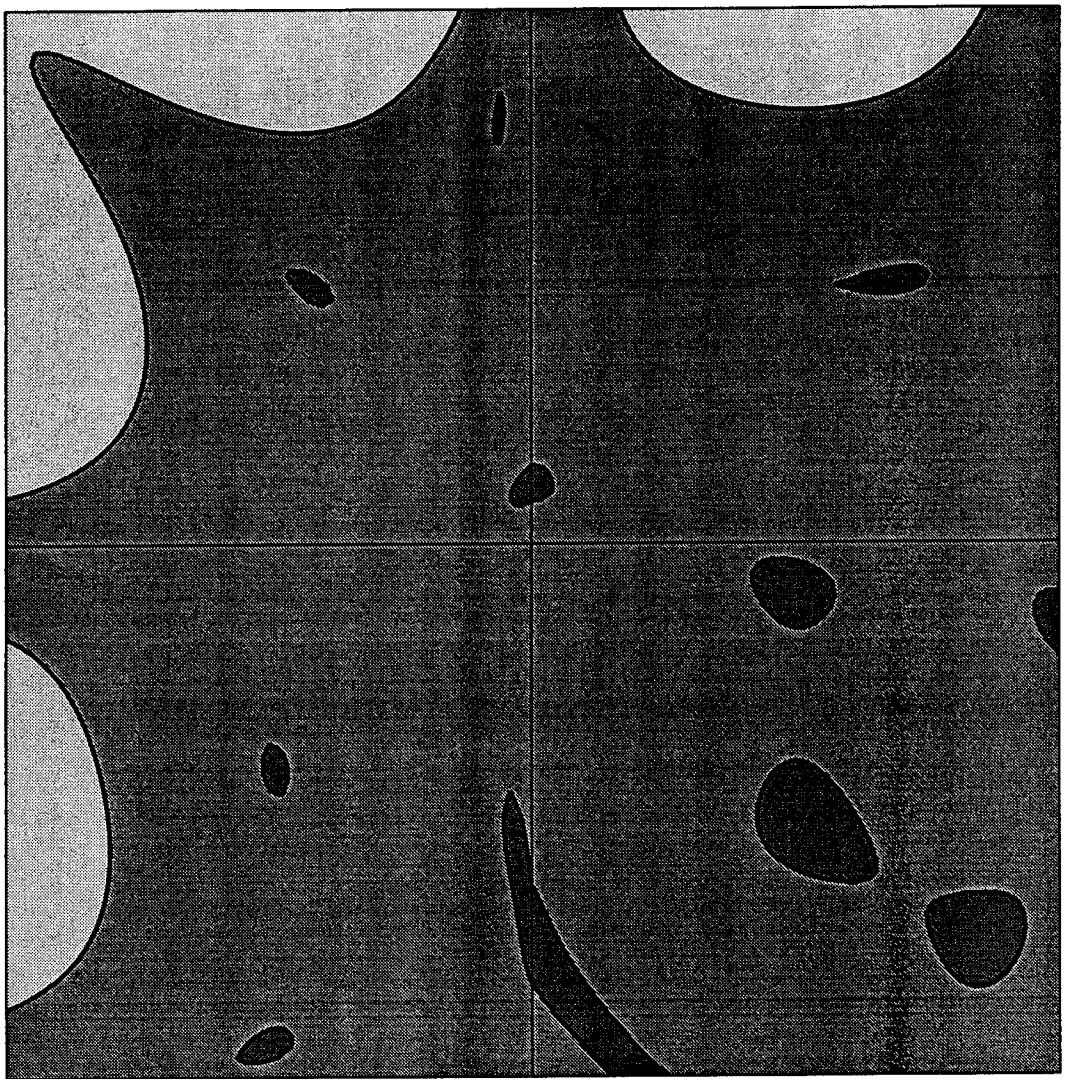
‖V2‖/eta = 19.13% , ZZ-error
Regions of 2.5% , 5% , 10%
MIN = 0.007 , MAX = 0.103

Fig. 10c

Fig. 11a
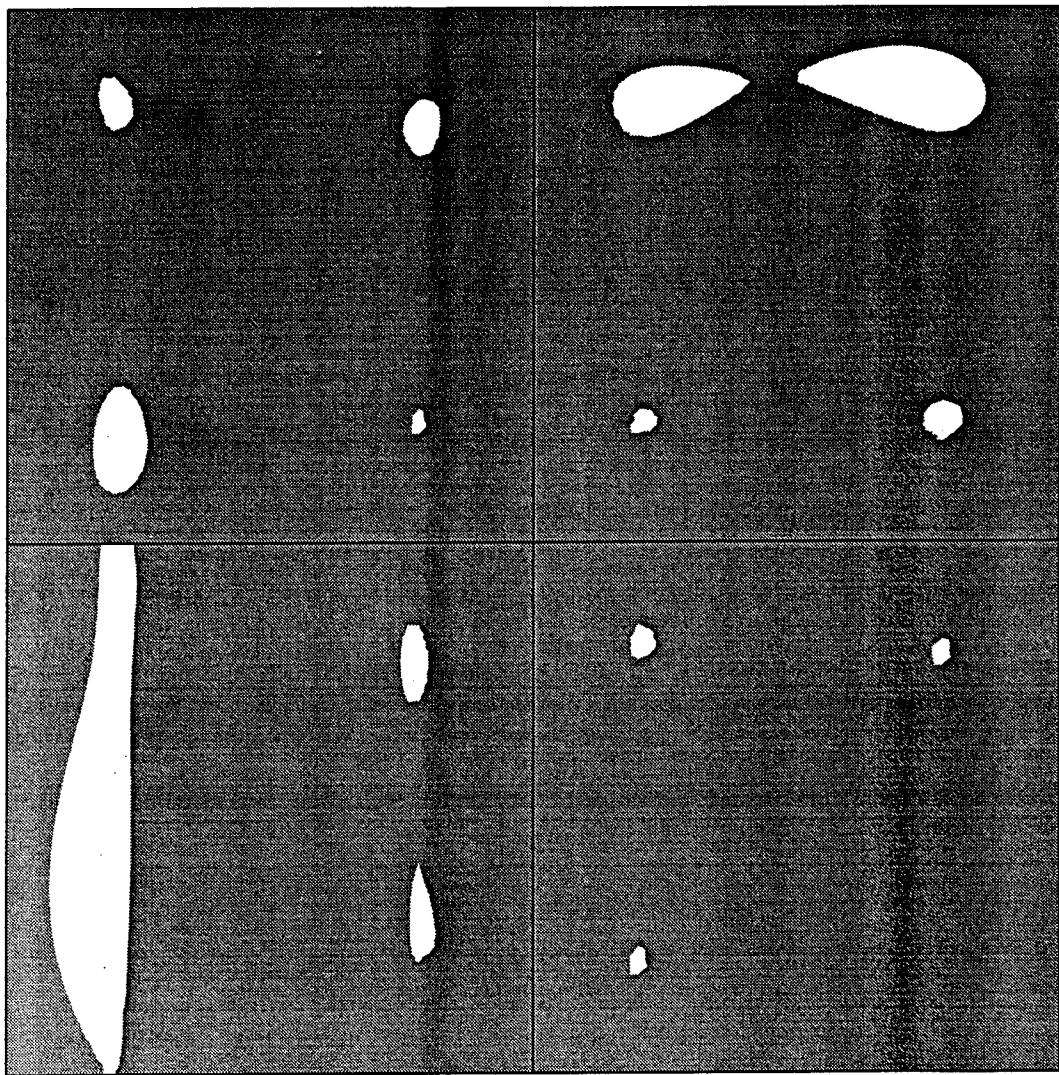
Fig. 11b
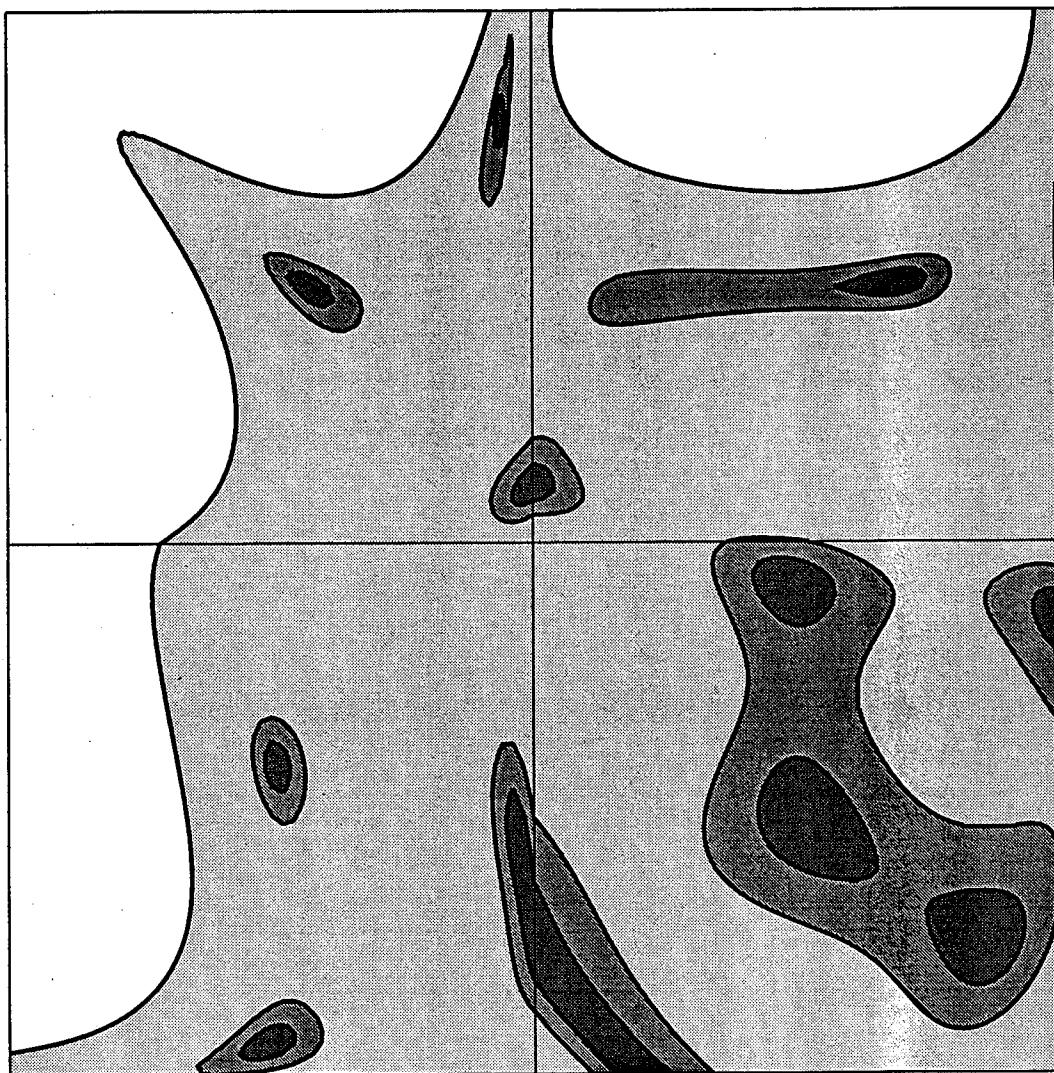
||V2||/eta = 44.60% , ZZ-error
Regions of 2.5% , 5% , 10%
MIN = 0.019 , MAX = 0.241

Fig. 12a
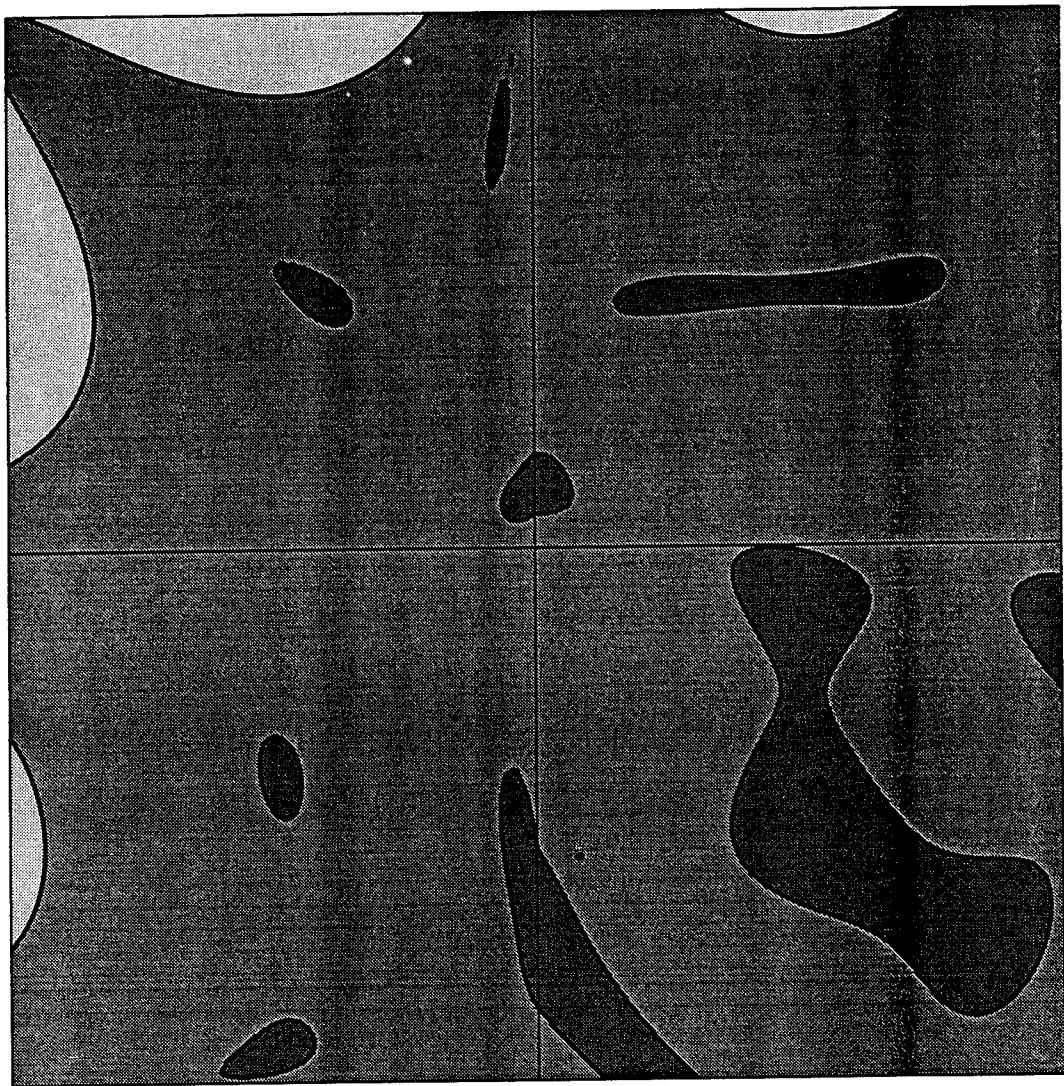
||V2||/eta = 11.77% , ZZ-error
Regions of 2.5% , 5% , 10%
MIN = 0.0004 , MAX = 0.081

Fig. 12b
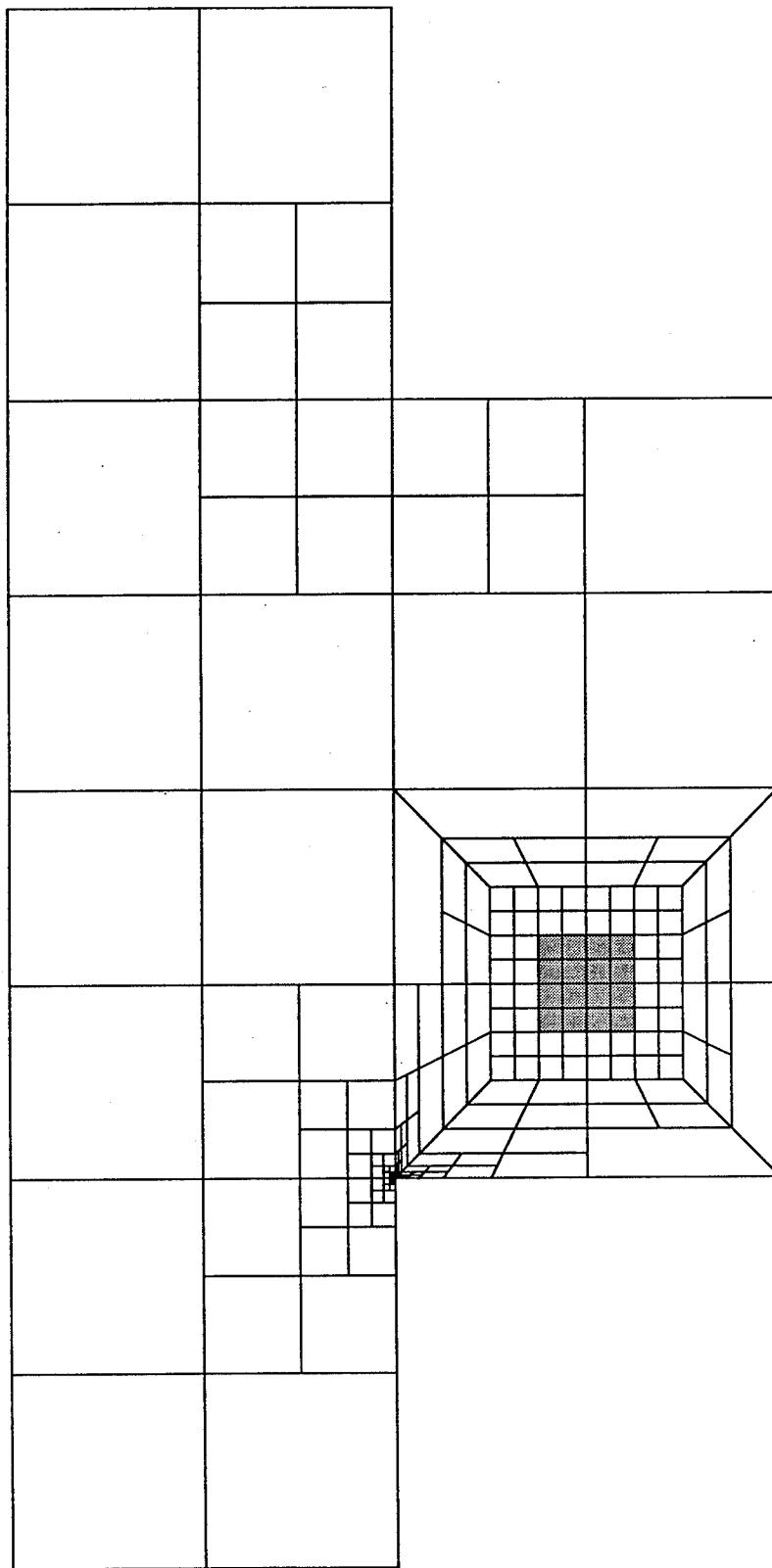
NDOF = 1393

Fig. 13a
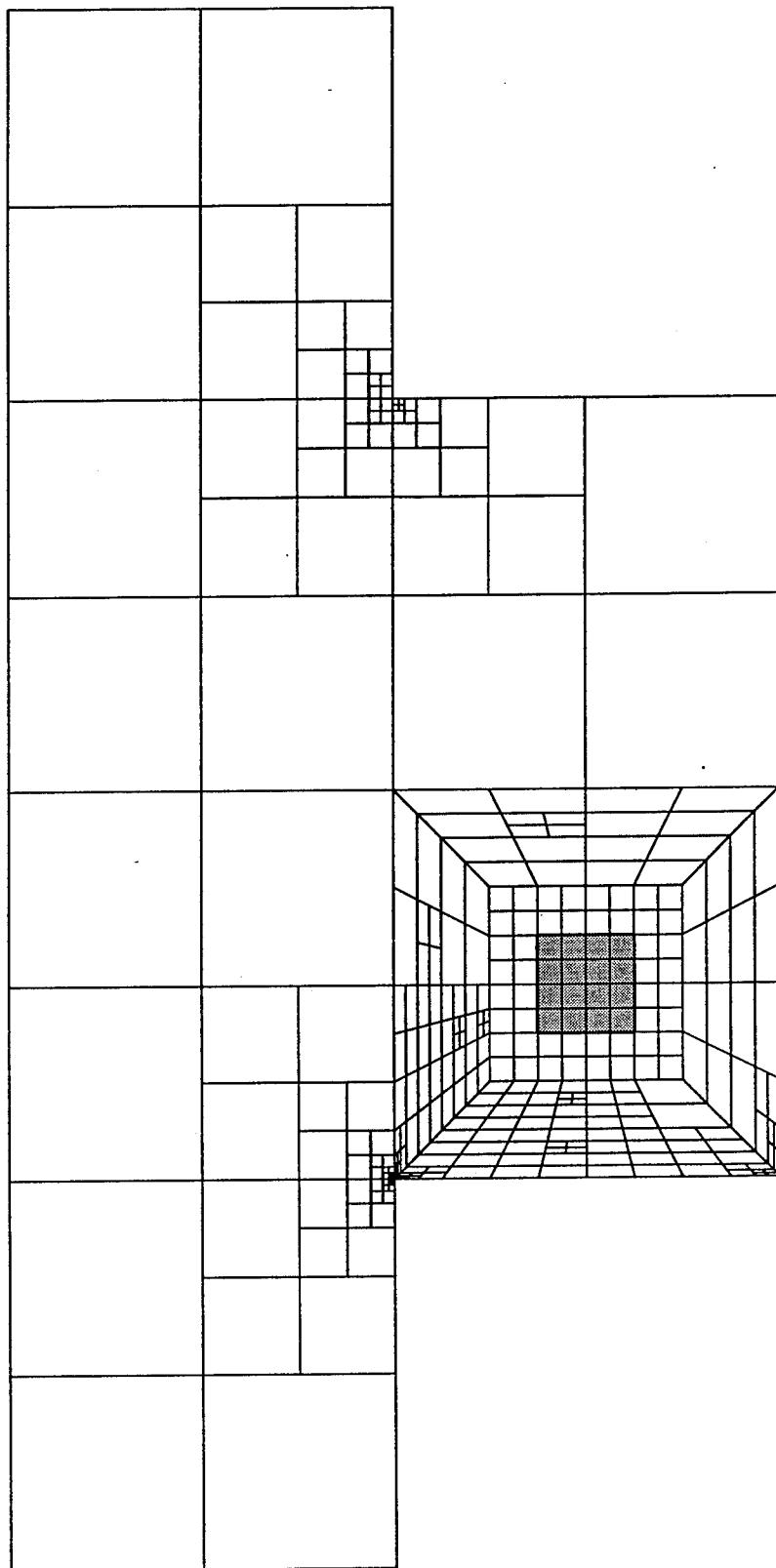
Fig. 13b

NDOF = 1861
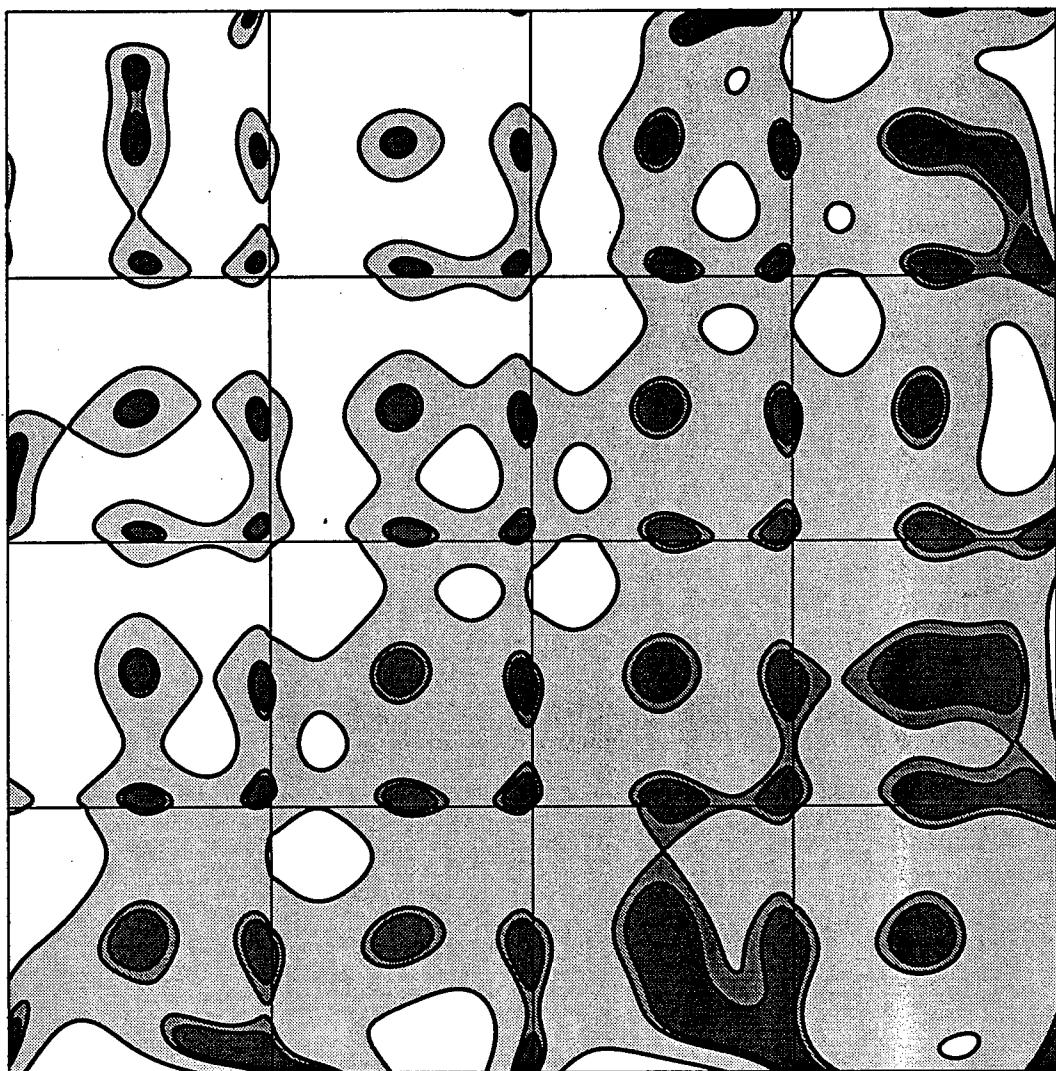
‖V2‖/eta = 7.76% , ZZ-error
Regions of 0.5% , 1% , 2%
MIN = 0.000004 , MAX = 0.033

Fig. 14a
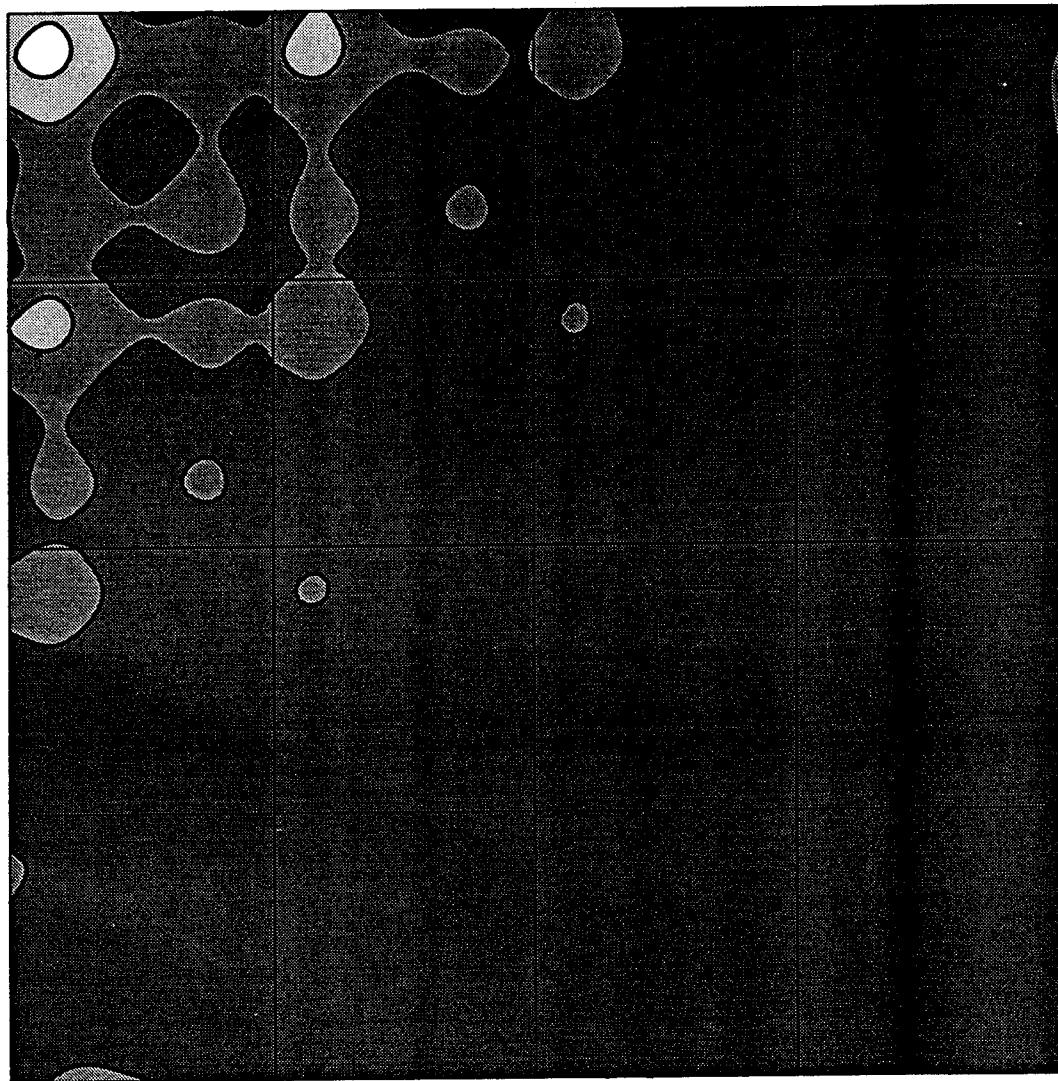
‖V2‖/eta = 4.48% , ZZ-error
Regions of 0.5% , 1% , 2%
MIN = 1.44E-7 , MAX = 0.021

Fig. 14b
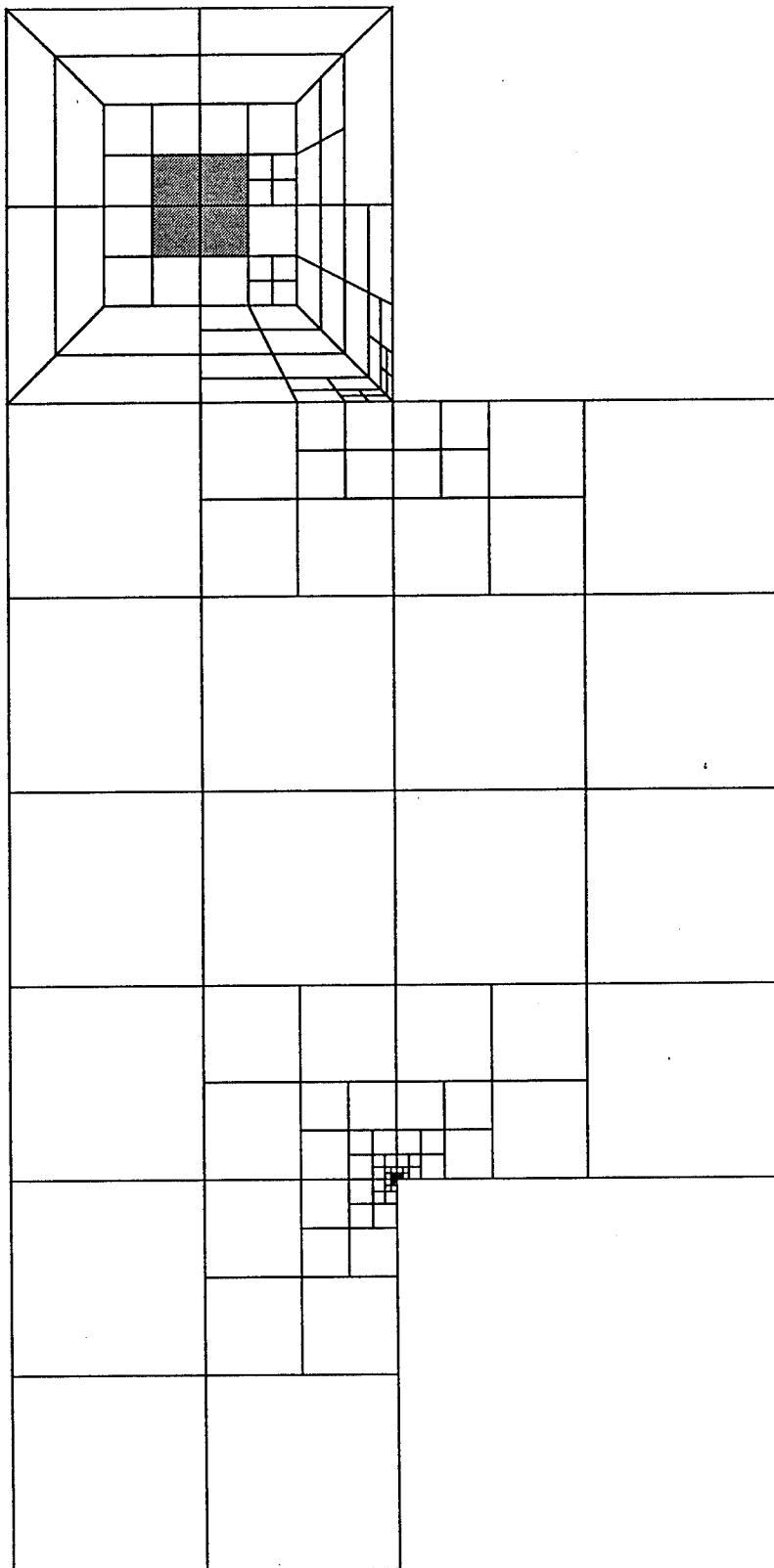
Fig. 15a

NDOF = 927
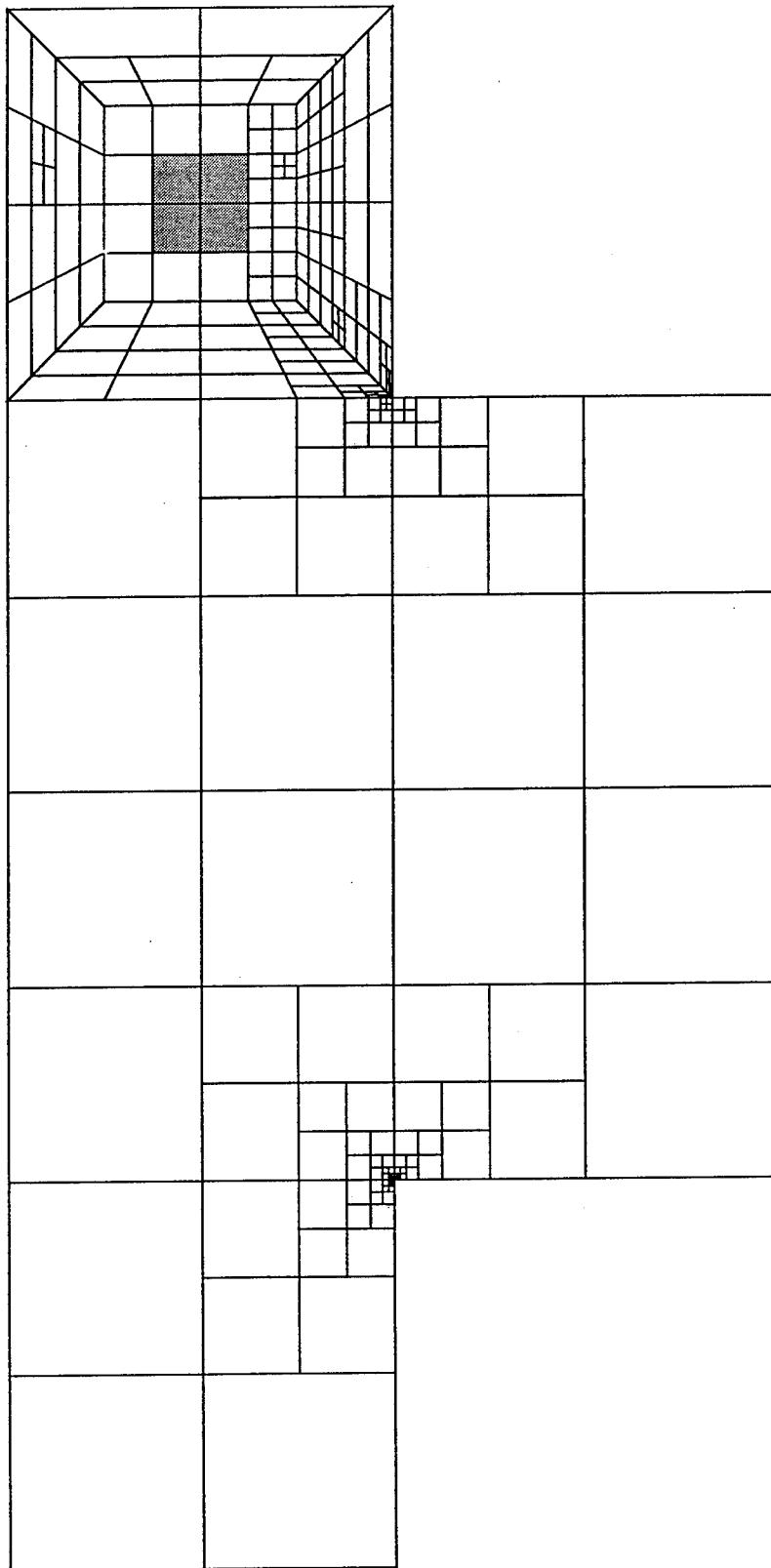
Fig. 15b

NDOF = 1345
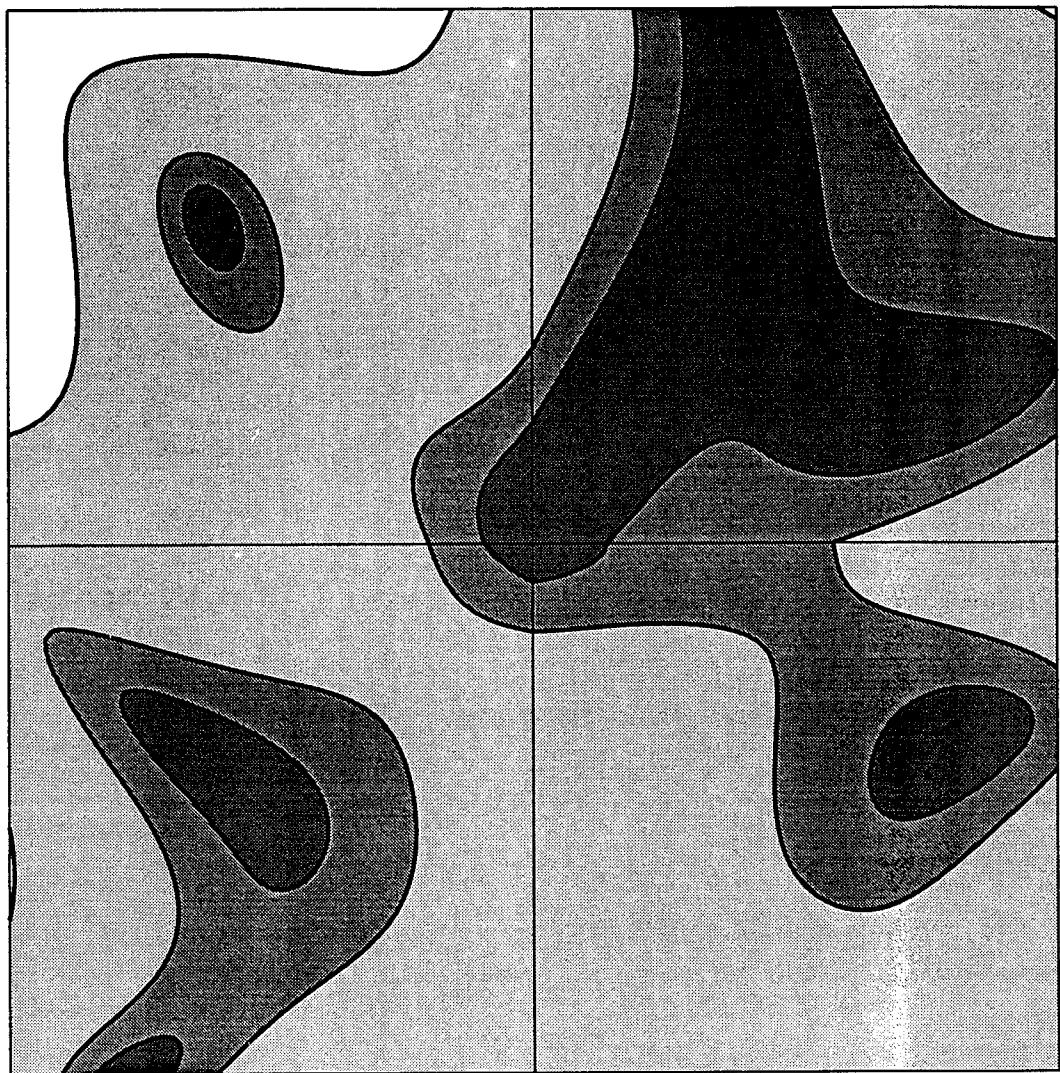
||V2||/eta = 5.79% , ZZ-error
Regions of 1.0% , 2% , 4%
MIN = 0.0003 , MAX = 0.043
Patch 2

Fig. 16a
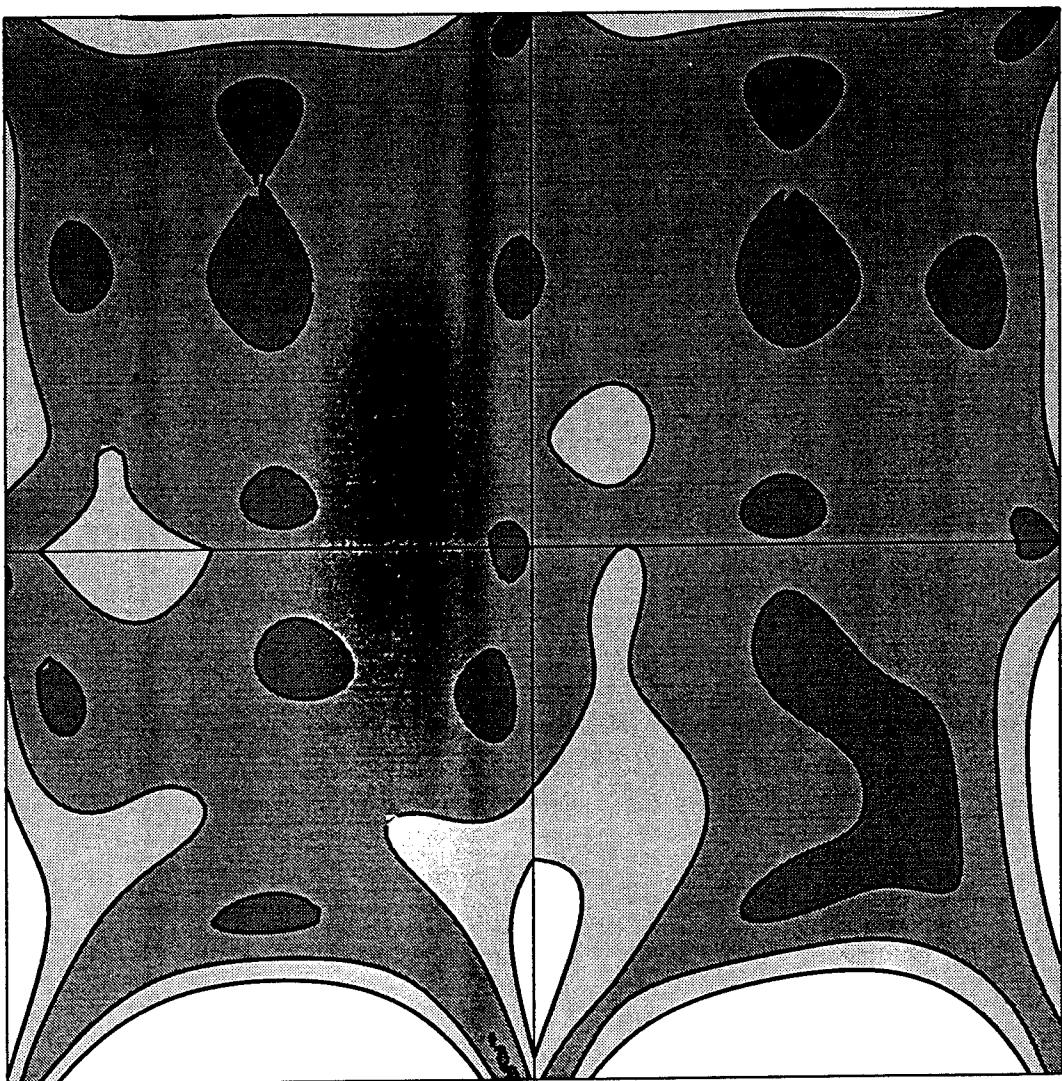
||V2||/eta = 1.73% , ZZ-error
Regions of 0.25% , 0.5% , 1.0%
MIN = 1.33E-7 , MAX = 0.014

Fig. 16b

The Laboratory for Numerical Analysis is an integral part of the Institute for Physical Science and Technology of the University of Maryland, under the general administration of the Director, Institute for Physical Science and Technology. It has the following goals:

To conduct research in the mathematical theory and computational implementation of numerical analysis and related topics, with emphasis on the numerical treatment of linear and nonlinear differential equations and problems in linear and nonlinear algebra.

To help bridge gaps between computational directions in engineering, physics, etc., and those in the mathematical community.

To provide a limited consulting service in all areas of numerical mathematics to the University as a whole, and also to government agencies and industries in the State of Maryland and the Washington Metropolitan area.

To assist with the education of numerical analysts, especially at the postdoctoral level, in conjunction with the Interdisciplinary Applied Mathematics Program and the programs of the Mathematics and Computer Science Departments. This includes active collaboration with government agencies such as the National Institute of Standards and Technology.

To be an international center of study and research for foreign students in numerical mathematics who are supported by foreign governments or exchange agencies (Fulbright, etc.).

Further information may be obtained from **Professor I. Babuška**, Chairman, Laboratory for Numerical Analysis, Institute for Physical Science and Technology, University of Maryland, College Park, Maryland 20742-2431.